QoS-Oriented Sensing-Communication-Control Co-Design for UAV-Enabled Positioning

QoS-Oriented Sensing-Communication-Control Co-Design for UAV-Enabled Positioning

Zijie Wang, Rongke Liu, *Senior Member, IEEE,* Qirui Liu, Lincong Han, Yuan Wu, *Senior Member, IEEE,* and John S. Thompson, *Fellow, IEEE*

Abstract

Unmanned aerial vehicle (UAV)-enabled positioning that uses UAVs as aerial anchor nodes has been envisioned as a promising solution for providing positioning services in harsh environments. In previous research, state sensing and control of UAVs was either ignored or assumed to be performed continuously, resulting in system instability or a waste of wireless resources. Therefore, in this paper, we propose a quality-of-service (QoS)-oriented sensing-communication-control (SCC) co-design scheme for UAV-enabled positioning systems. We first establish mathematical models of UAV state sensing and control. Then, we analyze the influence of sensing scheduling and transmission failure on the stability of UAV, as well as the performance of positioning services in the presence of UAV control error. Based on these models and analysis results, we further study the problem of minimizing the amount of data transmitted by optimizing the sensing scheduling and blocklength allocation under the condition of meeting each user's requirement on position accuracy. Finally, a heuristic algorithm is developed to solve this mixed-integer nonlinear problem. Numerical results demonstrate the validity and superiority of the proposed scheme. Compared with two benchmark schemes, our scheme reduces the failure rate or resource consumption of positioning services by more than 75% or 80%.

Index Terms

Unmanned aerial vehicle (UAV), UAV-enabled positioning, Sensing-communication-control (SCC) co-design, Quality-of-service (QoS).

Z. Wang, R. Liu, Q. Liu and L. Han are with the School of Electronic and Information Engineering, Beihang University, Beijing 100191, China (e-mail: wangmajie@buaa.edu.cn; rongke_liu@buaa.edu.cn).

Y. Wu is with the State Key Laboratory of Internet of Things for Smart City and the Department of Computer and Information Science, University of Macau, Macau 999078, China (e-mail: yuanwu@um.edu.mo).

J. S. Thompson is with the Institute for Digital Communications, School of Engineering, University of Edinburgh, King's Buildings, Edinburgh, EH9 3JL, U.K. (e-mail: john.thompson@ed.ac.uk).

I. INTRODUCTION

A. Motivation

Ubiquitous positioning has been widely recognized as an essential service and an enabling technology for both the current fifth generation (5G) wireless networks and the future sixth generation (6G) communications [1], [2]. Unfortunately, conventional wireless positioning technologies represented by the global navigation satellite system (GNSS) and cellular-based positioning may suffer severe performance degradation in some harsh environments due to frequent non-line-of-sight (NLoS) propagation and unsatisfactory geometry of available anchor nodes [3]–[6]. Unlike satellites and terrestrial BSs, unmanned aerial vehicles (UAVs) can be controlled to fly to places where they can establish line-of-sight (LoS) links with ground users [7]. In addition, by considering the UAV-user layout in the deployment of UAVs, the problem of poor geometry can also be addressed [8]. Because of the aforementioned advantages of UAVs, UAV-enabled positioning that uses UAVs as aerial anchor nodes has been envisioned as a promising solution for positioning in challenging environments [9], [10].

As a class of automated systems, the operation of UAV-enabled positioning systems requires appropriate design and coordination of sensing, communication and control (SCC) functions [11]. In existing systems, these three tasks were commonly designed separately and performed continuously [12]. Since wireless sensing and communication are implemented through signal transmission and reception, the current design of SCC functions may expend a large amount of radio resources and UAV onboard energy [13]. Recently, many studies pointed out that considering the cooperation of SCC functions at the beginning of system design, namely SCC co-design, can help improve system performance or resource efficiency [14], [15], making it a potential solution for the problems mentioned above. However, there are two major challenges need to be tackled before applying SCC co-design to UAV-enabled positioning: 1) a lack of a general framework for describing the relationship between the design of SCC functions and position accuracy; 2) the UAVs are coupled to each other since the positioning of each user requires the cooperation between multiple UAVs. The aim of this paper is to tackle these two challenges and develop a practical SCC co-design scheme for UAV-enabled positioning.

B. Related Work

Due to their high flexibility and adaptability in harsh environments, unmanned aerial vehicles (UAV) have recently received considerable attention from the research community and may help

create a whole new paradigm for wireless networks [16]. In the past few years, researchers have studied the potential of UAVs as aerial BSs to establish emergency networks or realize secure transmission [17], [18]. In addition to their use for communication, UAV can also provide wireless positioning services for ground users, that is, UAV-enabled positioning. Sallouha *et al.* [19] proposed a system that utilizes UAVs and the received-signal-strength (RSS) technique to locate ground users, and studied the trade-off between position accuracy and propulsion energy consumption [20]. Wang *et al.* [10] introduced the time-difference-of-arrival (TDoA) approach into UAV-enabled positioning and realized high-accuracy, three-dimensional (3-D) localization by exploiting the vertical diversity of UAV platforms. In these studies, UAVs were leveraged as the anchor nodes with perfect knowledge of their own positions. In practice, UAVs' positions are obtained through state sensing, and the inevitable sensing errors will cause uncertainty in anchor position information [21], [22]. Thus, the authors in [21] studied the problem of UAV self-localization and evaluated the impact of UAV position uncertainty on positioning performance. Moreover, Liu *et al.* [22] proposed a deployment optimization method to improve the accuracy of UAV-enabled positioning whole considering UAV position uncertainty. These two studies assume that UAVs can hover stably at fixed positions, which is difficult to achieve in practice due to the influence of environmental factors like the wind [23]. Hence, the authors in [24] quantitatively analyzed the influence of the instability of UAV platforms on UAV relative localization. Nevertheless, in [24], the anchor position uncertainty in different directions caused by UAV instability was modeled as independent Gaussian random variables with the same variance, which may be too optimistic for practice.

In terms of the co-design of different functions, several successful attempts have been made in recent years. Liu *et al.* [25] integrated radar sensing and millimeter wave (mmWave) communication functions into a multiple-input multiple-output (MIMO) system. In [25], the users or targets of the two functions are different, which means that a single user cannot benefit from both functions. In [26], the vehicle motion predicted through radar sensing was used to assist the reception of downlink communication signals. Nevertheless, control issues that are critical in vehicle applications are not considered in this research. Mei *et al.* [27] and González *et al.* [28] introduced the co-design of communication and control into vehicle-to-vehicle (V2V) networks, and developed resource scheduling algorithms to ensure the so-called *string stability* of vehicle platoons. In these two studies, the sensing of each vehicle's kinematic status is assumed to be performed perfectly without failures or errors, which is not realistic for real-world applications.

In [14] and [29], control-aware communication was used to improve the resource efficiency of wireless control systems. These two studies focused on the stability and resource consumption of control systems, rather than the system's ability to perform the required tasks. In fact, a system may not need to be very stable to provide services that satisfy users' demands, and over-stringent stability requirements may waste resources.

From the above analysis, it can be concluded that if we want to improve the performance or efficiency of UAV-enabled positioning systems through the joint design of multiple functions, the following requirements need to be met: 1) the SCC functions in each UAV should be considered comprehensively; 2) the imperfections of each function should be modeled objectively; 3) the main consideration should be the performance of positioning services.

C. Main Contributions

In this paper, a quality-of-service (QoS)-oriented SCC co-design scheme is proposed to improve the resource efficiency of UAV-enabled positioning while ensuring that users' requirements on position accuracy are met. Specifically, the mathematical models of UAV state sensing and control in two operation modes, "open-loop (OL)" and "closed-loop (CL)", are first established. Based on these models, we further analyze the UAV stability in different operation modes, as well as the position accuracy of ground users in the presence of UAV position uncertainty. The analysis results indicate that the position accuracy is mainly determined by UAVs' operation modes, which in this study depends on the scheduling of UAV state sensing and successful transmissions of sensing data with finite blocklength. Then, we formulate the problem of reducing the resource consumption of positioning services through sensing scheduling and blocklength allocation as a mixed-integer nonlinear optimization problem, and develop a heuristic algorithm to solve it.

The major contributions of this paper are listed as follows:

- The proposed co-design scheme provides a mathematical model for the relationship between the design of SCC functions and the quality of positioning services, which can be used as a general framework for future research on SCC co-design in UAV-enabled positioning.
- The proposed heuristic algorithm decouples the constraint on position accuracy into constraints on each UAV's control error, making it suitable for large-scale systems.

Numerical results demonstrate that our proposed scheme achieves significantly lower failure rate or better resource efficiency compared with the benchmark schemes. To the best of our knowledge, this work is the first to introduce the SCC co-design into UAV-enabled positioning.

The remainder of this paper is organized as follows. Section II introduces the system model. Section III analyzes the influence of SCC functions on position accuracy and formulates the optimization problem. The proposed heuristic algorithm is presented in Section IV. Section V provides numerical results, and Section VI concludes this paper.

Notations: Lowercase and uppercase boldface letters ($\mathbf{x}$ and $\mathbf{X}$) represent column vectors and matrices, respectively. The superscript T indicates the transpose operation ($\mathbf{X}^T$) and superscript -1 indicates matrix inverse ($\mathbf{X}^{-1}$). $\|\cdot\|_2$ and $\mathrm{tr}\,(\cdot)$ denote the Euclidean norm and matrix trace, respectively. $E\{\cdot\}$ represents the statistical expectation operator and $P(\cdot)$ indicates the probability. $\mathrm{diag}\,(\cdot)$ and $\mathrm{blkdiag}\,(\cdot)$ denote the diagonal and block diagonal matrices, respectively. $\mathbf{I}_N$ is the $N \times N$ identity matrix and $\mathbf{0}_{N\times M}$ represents the $N \times M$ all-zero matrix. $\dot{v}$ indicates the first-order derivative of the time-dependent function v with respect to time.

II. System Model

In this paper, as shown in Fig. 1(a), we consider a scenario where multiple ground users requiring positioning services are located in an urban environment. In such an environment, conventional technologies such as GNSS systems and terrestrial cellular-based positioning fail to meet users' requirements. Therefore, a UAV-enabled positioning system consisting of multiple low-altitude UAV platforms undertakes the task of locating ground users. The UAVs used can be classified into two groups according to their functions, namely the "agent UAV (UAV-A)" and "beacon UAV (UAV-B)". The UAV-As are deployed close to users as they are responsible for locating user equipment (UE) through LoS links. Similar to UE, UAV-As deployed in GNSS-challenged environment are unable to determine their own locations through GNSS systems. Moreover, it is difficult for UAV-As to establish LoS links with terrestrial BSs due to their long distance from BSs. So, the positioning services provided by terrestrial BSs are severely affected by the NLoS propagation of positioning signals and cannot achieve the desired position accuracy of UAV-As. On the contrary, the air-to-air (A2A) channels between different UAVs are generally dominated by the LoS components [30], which means that the relative range measurements obtained in A2A channels are more likely to achieve high position accuracy. Thus, UAV-Bs whose locations have been accurately estimated are introduced into the considered scenario and are used to provide UAV-As with relative range measurements required for state sensing.

The considered UAV-enabled positioning system consists of N_A UAV-As, N_B UAV-Bs and M UEs. UAV-As and UAV-Bs are denoted by sets $\mathcal{N}_A = \{1, \cdots, N_A\}$ and $\mathcal{N}_B = \{1, \cdots, N_B\}$,

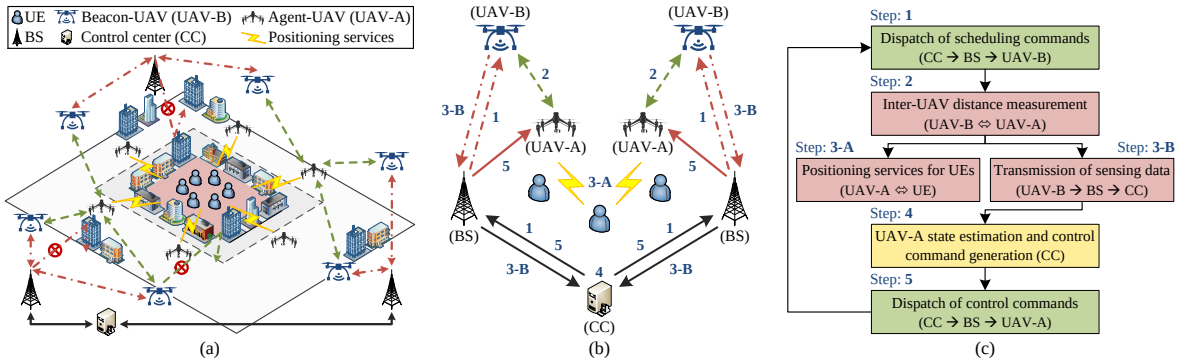

Fig. 1. (a) Deployment environment, (b) structure and (c) operation strategy of the considered UAV-enabled positioning system.

respectively. The j-th UAV-A ($j \in \mathcal{N}_A$) is deployed at a carefully selected hovering point (HP), which can be denoted by the horizontal coordinates $\mathbf{q}_j^{\circ} \in \mathbb{R}^{2\times 1}$ and height h_v. The 3-D coordinates of j-th UAV-A's HP are denoted by $\mathbf{q}_j^{\circ,3D} = \left[\left(\mathbf{q}_j^{\circ}\right)^T, h_v\right]^T \in \mathbb{R}^{3\times 1}$. It is assumed that UAV-As can maintain the preset altitude, while their horizontal locations are time-varying due to environmental factors like wind. Then, we represent the true location of the j-th UAV-A in time slot t as $\mathbf{q}_{j,t} \in \mathbb{R}^{2\times 1}$ ($\mathbf{q}_{j,t}^{3D} = \left[\left(\mathbf{q}_{j,t}\right)^T, h_v\right]^T \in \mathbb{R}^{3\times 1}$). UAV-Bs fly at the same altitude (h_v) as UAV-As, and the location of the i-th UAV-B ($i \in \mathcal{N}_B$) is denoted by $\mathbf{b}_i \in \mathbb{R}^{2\times 1}$ ($\mathbf{b}_i^{3D} = \left[\left(\mathbf{b}_i\right)^T, h_v\right]^T \in \mathbb{R}^{3\times 1}$). UEs are represented by the set $\mathcal{M} = \{1, \cdots, M\}$, and the true location of the m-th UE ($m \in \mathcal{M}$) is denoted as $\mathbf{p}_m \in \mathbb{R}^{2\times 1}$ ($\mathbf{p}_m^{3D} = \left[\left(\mathbf{p}_m\right)^T, 0\right]^T \in \mathbb{R}^{3\times 1}$).

Fig. 1(b) and (c) show the structure and operation strategy of the considered system, respectively. Specifically, at the beginning of each time slot, the control center (CC) sends scheduling commands to the UAV-Bs (step 1 in Fig. 1). The scheduling commands contain the indexes of the UAV-As that require state sensing and the blocklength for the transmission of sensing data. UAV-Bs then measure their relative distances to the scheduled UAV-As, and collect velocity and acceleration measurements from UAV-As' onboard sensors (step 2). Subsequently, UAV-As provide positioning services to UEs (step 3-A), while the UAV-Bs transmit sensing data to BSs and CC with the specified blocklength (step 3-B). The reason for using finite blocklength transmission is that the sensing data is used for UAV state estimation and control, which is delay-sensitive and safety-critical [31]. After receiving the sensing data, CC estimates the state of each UAV-A and generates the control input command (step 4). There are two reasons for choosing CC to perform state estimation: 1) all UAVs in the considered system are low-cost mini-UAVs, whose onboard computational power are insufficient for estimation algorithms with relatively

high complexity such as maximum-likelihood (ML) estimation; 2) since each UE is served by multiple UAV-As, the scheduling command and control input command of each UAV-A should be generated according to the states of other UAV-As, which are unavailable for a single UAV. Finally, CC sends control commands to UAV-As, and each UAV-A adjusts its state according to the received command (step 5). Due to the large transmit power of BSs, the failure rates of the command transmission in steps 1 and 5 are far lower than those of the data transmission in step 3-B [14]. For simplicity, in this paper, the command transmission in the considered system is assumed to be perfect, and transmission failures occur only in step 3-B.

In the following subsections, we provide the technical details of the considered system.

A. Model of UAV State Sensing

Denote the j-th UAV-A's velocity and acceleration in time slot t as $\mathbf{v}_{j,t}=\left[v_{j,t}^{(x)}, v_{j,t}^{(y)}\right]^T \in \mathbb{R}^{2\times 1}$ and $\mathbf{a}_{j,t}=\left[a_{j,t}^{(x)}, a_{j,t}^{(y)}\right]^T \in \mathbb{R}^{2\times 1}$, respectively. Then, the true state of this UAV-A can be represented by vector $\mathbf{x}_{j,t} = \left[\Delta\mathbf{q}_{j,t}^T, \mathbf{v}_{j,t}^T, \mathbf{a}_{j,t}^T\right]^T \in \mathbb{R}^{6\times 1}$, where $\Delta\mathbf{q}_{j,t}=\left[\Delta q_{j,t}^{(x)}, \Delta q_{j,t}^{(y)}\right]^T=\mathbf{q}_{j,t}-\mathbf{q}_j^{\circ}$.

In order to estimate UAV-As' locations, the well-known two-way ranging (TWR) technique is used to measure the inter-UAV distances between UAV-As and UAV-Bs. Compared with TDoA and other positioning techniques used in terrestrial networks, TWR technique can ease the constraint of clock synchronization through the exchange of messages, making it suitable for mobile anchor nodes like UAVs [32]. As derived in [8], the relative range measurement corresponding to the j-th UAV-A and i-th UAV-B can be written as

$$\hat{d}_{j,t}^i = d_{j,t}^i + n_{d,j,t}^i = \left\|\mathbf{q}_{j,t}^{3D} - \mathbf{b}_i^{3D}\right\|_2 + n_{d,j,t}^i, \tag{1}$$

where $d_{j,t}^i = \left\|\mathbf{q}_{j,t}^{3D} - \mathbf{b}_i^{3D}\right\|_2$ denotes the true distance between these two UAVs; $n_{d,j,t}^i \sim \mathcal{N}\left(0, \sigma_d^2\right)$ is the distance measurement error caused by clock drift between the UAVs' local clocks, and σ_d^2 is its variance. As mentioned in [8], the value of σ_d^2 is mainly determined by the crystal tolerance of the UAV's oscillator and the response delay of TWR. Since UAVs in the considered system use the same type of oscillators and the same TWR protocol, all inter-UAV distance measurements have the same variance for σ_d^2.

For each UAV-A j, three UAV-Bs are assigned to sense its state, denoted by the set $\mathcal{N}_B^{A_j}$ ($\mathcal{N}_B^{A_j} \in \mathcal{N}_B$). Then, the three inter-UAV distance measurements corresponding to the j-th UAV-A can be denoted by the following vector:

$$\hat{\mathbf{d}}_{j,t} = \left[\cdots, \hat{d}_{j,t}^i, \cdots\right]^T = \mathbf{d}_{j,t} + \mathbf{n}_{\mathbf{d},j,t}, \quad i \in \mathcal{N}_B^{A_j}, \tag{2}$$

where $\mathbf{d}_{j,t} = \left[\cdots, d_{j,t}^{i}, \cdots\right]^T$ ($i \in \mathcal{N}_B^{A_j}$); $\mathbf{n}_{\mathbf{d},j,t} = \left[\cdots, n_{d,j,t}^{i}, \cdots\right]^T$ is the noise vector consisting of mutually independent measurement errors with same variance. Thus, the covariance matrix of $\mathbf{n}_{\mathbf{d},j,t}$ can be expressed as $\mathbf{R}_{\mathbf{d}} = \sigma_d^2 \cdot \mathbf{I}_3$.

With the above measurement equations, the j-th UAV-A's location in time slot t can be estimated by CC through the ML method. Then, the Cramér-Rao lower bound (CRLB) that can be approached by the ML method is used to indicate the accuracy of the estimation of UAV-As' locations, which can be expressed as

$$\mathrm{CRLB}\left(\mathbf{q}_{j,t}\right) = \left(\mathbf{H}_j^T \mathbf{R}_{\mathbf{d}}^{-1} \mathbf{H}_j\right)^{-1} = \sigma_d^2 \cdot \left(\mathbf{H}_j^T \mathbf{H}_j\right)^{-1}, \tag{3}$$

where $\mathbf{H}_j$ is the Jacobian matrix of equation (2) at $\mathbf{q}_{j,t}$, and

$$\mathbf{H}_j = \partial \mathbf{d}_{j,t} / \partial \mathbf{q}_{j,t} = \left[\cdots, \mathbf{h}_j^i\left(\mathbf{q}_{j,t}\right), \cdots\right]^T = \left[\cdots, \left(\mathbf{q}_{j,t} - \mathbf{b}_i\right) / \left\|\mathbf{q}_{j,t}^{3D} - \mathbf{b}_i^{3D}\right\|_2, \cdots\right]^T,\ i \in \mathcal{N}_B^{A_j}. \tag{4}$$

It is noteworthy that with an appropriate control strategy, the deviation between the UAV-A's true location ($\mathbf{q}_{j,t}$) and the corresponding HP ($\mathbf{q}_j^{\circ}$) is acceptable, and its influence on the geometry of UAVs is negligible [33]. Thus, equation (4) can be approximated by replacing $\mathbf{q}_{j,t}$ with $\mathbf{q}_j^{\circ}$.

We assume that the estimation of the UAV-As' locations could approach the CRLB. Then, the covariance matrix of UAV-A location estimate ($\hat{\mathbf{q}}_{j,t}$) can be expressed as $\mathbf{R}_{\mathbf{q},j} \approx \mathrm{CRLB}\left(\mathbf{q}_{j,t}\right)$. Utilizing the relationship $\Delta\mathbf{q}_{j,t} = \mathbf{q}_{j,t} - \mathbf{q}_j^{\circ}$, the estimate of $\Delta\mathbf{q}_{j,t}$ can be written as

$$\Delta\hat{\mathbf{q}}_{j,t} = \hat{\mathbf{q}}_{j,t} - \mathbf{q}_j^{\circ} = \Delta\mathbf{q}_{j,t} + \mathbf{n}_{\Delta\mathbf{q},j,t}, \tag{5}$$

where $\mathbf{n}_{\Delta\mathbf{q},j,t} \sim \mathcal{N}(\mathbf{0}_{2\times 1}, \mathbf{R}_{\Delta\mathbf{q},j})$ is the estimation error, and $\mathbf{R}_{\Delta\mathbf{q},j} = \mathbf{R}_{\mathbf{q},j}$ is its covariance matrix.

In addition, while measuring the inter-UAV distances, the UAV-As also send their velocity and acceleration measurements to the UAV-Bs by embedding them into the response message. The velocity and acceleration of the j-th UAV-A measured in time slot t can be expressed as

$$\hat{\mathbf{v}}_{j,t} = \mathbf{v}_{j,t} + \mathbf{n}_{\mathbf{v},j,t}, \qquad \hat{\mathbf{a}}_{j,t} = \mathbf{a}_{j,t} + \mathbf{n}_{\mathbf{a},j,t}, \tag{6}$$

where $\mathbf{n}_{\mathbf{v},j,t} \sim \mathcal{N}\left(\mathbf{0}_{2\times 1}, \mathbf{R}_{\mathbf{v}}\right)$ and $\mathbf{n}_{\mathbf{a},j,t} \sim \mathcal{N}\left(\mathbf{0}_{2\times 1}, \mathbf{R}_{\mathbf{a}}\right)$ denote measurement errors, and their covariance matrices ($\mathbf{R}_{\mathbf{v}}$ and $\mathbf{R}_{\mathbf{a}}$) are unchanged among UAV-As.

Then, the sensing result of the j-th UAV-A's state in time slot t can be written as:

$$\hat{\mathbf{x}}_{j,t} = \left[\Delta\hat{\mathbf{q}}_{j,t}^T, \hat{\mathbf{v}}_{j,t}^T, \hat{\mathbf{a}}_{j,t}^T\right]^T = \mathbf{x}_{j,t} + \boldsymbol{\eta}_{j,t}, \tag{7}$$

where $\boldsymbol{\eta}_{j,t} = \left[\mathbf{n}_{\Delta\mathbf{q},j,t}, \mathbf{n}_{\mathbf{v},j,t}, \mathbf{n}_{\mathbf{a},j,t}\right]^T \sim \mathcal{N}\left(\mathbf{0}_{6\times 1}, \mathbf{R}_{\boldsymbol{\eta},j}\right)$ is the noise vector consisting of three kinds of mutually independent measurement errors, and its covariance matrix can be expressed as

$$\mathbf{R}_{\boldsymbol{\eta},j} = \mathrm{blkdiag}\left(\mathbf{R}_{\Delta\mathbf{q},j}, \mathbf{R}_{\mathbf{v}}, \mathbf{R}_{\mathbf{a}}\right). \tag{8}$$

B. Model of UAV Control

For simplicity and without loss of generality, we consider the state of each UAV-A in the considered system as a linear time-invariant discrete-time system, whose dynamics model is given by

$$\mathbf{x}_{j,t+1} = \mathbf{A}_j \mathbf{x}_{j,t} + \mathbf{B}_j \mathbf{u}_{j,t} + \mathbf{w}_{j,t}, \tag{9}$$

where $\mathbf{A}_j \in \mathbb{R}^{6\times 6}$ and $\mathbf{B}_j \in \mathbb{R}^{6\times 2}$ are the state matrix and input matrix of the j-th UAV-A, respectively; $\mathbf{u}_{j,t} = \left[u_j^{(x)}, u_j^{(y)}\right]^T \in \mathbb{R}^{2\times 1}$ is the control input, i.e., the commanded acceleration; $\mathbf{w}_{j,t} \sim \mathcal{N}\left(\mathbf{0}_{6\times 1}, \mathbf{Q}_{\mathbf{w}}\right)$ is independent identically distributed (i.i.d.) process noise that characterizes the body jittering of UAV-As caused by environmental factors like the wind. The expressions for the matrices $\mathbf{A}_j$, $\mathbf{B}_j$ and $\mathbf{Q}_{\mathbf{w}}$ are derived in Appendix A.

As a linear system, UAV-A's control input vector can be determined using the state feedback law $\mathbf{u}_{j,t} = \mathbf{K}_j \mathbf{x}_{j,t}$, where $\mathbf{K}_j \in \mathbb{R}^{2\times 6}$ is the gain matrix. Then, equation (9) can be rewritten as

$$\mathbf{x}_{j,t+1} = \left(\mathbf{A}_j + \mathbf{B}_j \mathbf{K}_j\right) \mathbf{x}_{j,t} + \mathbf{w}_{j,t}. \tag{10}$$

Please note that the true state ($\mathbf{x}_{j,t}$) in the above equation is unavailable in practice. Therefore, the CC can only generate the control input ($\mathbf{u}_{j,t}$) based on state sensing or prediction results. If the sensing data is successfully received by CC, the control input will be generated in CL mode based on the estimated state ($\hat{\mathbf{x}}_{j,t}$), i.e., $\mathbf{u}_{j,t}^{(c)} = \mathbf{K}_j \hat{\mathbf{x}}_{j,t} = \mathbf{K}_j \left(\mathbf{x}_{j,t} + \boldsymbol{\eta}_{j,t}\right)$. Otherwise, the UAV-A will be controlled in OL mode and the control input is generated based on the predicted state. According to equation (10), if the last successful state sensing was performed in time slot $t - \Delta t_j^c$, the prediction of the UAV-A's state in time slot t can be expressed as

$$\bar{\mathbf{x}}_{j,t}^{\left(\Delta t_j^c\right)} = \left(\mathbf{A}_j + \mathbf{B}_j \mathbf{K}_j\right)^{\Delta t_j^c} \hat{\mathbf{x}}_{j,t-\Delta t_j^c} = \left(\mathbf{A}_j + \mathbf{B}_j \mathbf{K}_j\right)^{\Delta t_j^c} \left(\mathbf{x}_{j,t-\Delta t_j^c} + \boldsymbol{\eta}_{j,t-\Delta t_j^c}\right). \tag{11}$$

Then, the control input generated in OL mode can be written as $\mathbf{u}_{j,t}^{(o)} = \mathbf{K}_j \bar{\mathbf{x}}_{j,t}^{\left(\Delta t_j^c\right)}$, and the UAV-A's dynamics model for the two operation modes can be expressed as

$$\begin{aligned} \mathbf{x}_{j,t+1}^{(c)} &= \left(\mathbf{A}_j + \mathbf{B}_j \mathbf{K}_j\right) \mathbf{x}_{j,t} + \left(\mathbf{B}_j \mathbf{K}_j \boldsymbol{\eta}_{j,t} + \mathbf{w}_{j,t}\right), \quad \text{closed-loop}, \\ \mathbf{x}_{j,t+1}^{(o)} &= \mathbf{A}_j \mathbf{x}_{j,t} + \mathbf{B}_j \mathbf{K}_j \bar{\mathbf{x}}_{j,t}^{\left(\Delta t_j^c\right)} + \mathbf{w}_{j,t}, \qquad \text{open-loop}, \end{aligned} \tag{12}$$

where superscripts (c) and (o) indicate the CL and OL modes, respectively.

Furthermore, the update rule for parameter Δt_j^c in two operation modes is given by

$$\Delta t_j^c \leftarrow \begin{cases} 1, & \text{closed-loop}, \\ \Delta t_j^c + 1, & \text{open-loop}. \end{cases} \tag{13}$$

The CL and OL modes considered in this paper are the two most common operation modes in wireless control systems [14]. The major difference between these two operation modes is the basis for generating the control input of each UAV-A. Specifically, as mentioned above, the control inputs in CL and OL modes are generated based on UAV-A's estimated and predicted states, respectively. Due to the existence of unknown process noise ($\mathbf{w}_{j,t}$) in UAV-A's dynamics model, the predicted state will deviate significantly from UAV-A's true state after several consecutive time slots of OL control, resulting in incorrect control input. Thus, UAV-As in the considered system cannot maintain long-term stability in OL mode, and need to be frequently controlled in CL mode to maintain themselves in close vicinity of the corresponding HPs. However, it is noteworthy that the using of OL mode helps to reduce resource consumption in a sense, as it allows UAV-As not to perform state sensing. Thus, in the considered system, UAV-As' operation modes in each time slot should be carefully chosen according to UAV-As' stability and the overall resource consumption.

C. Model of Positioning Services for UE

Similar to the UAV state sensing, UAV-As also use the TWR technique to provide positioning services for UEs. Then, the distance measurement corresponding to the m-th UE and j-th UAV-A can be expressed as

$$\hat{r}_{m,t}^{j} = r_{m,t}^{j} + n_{r,m,t}^{j} = \left\|\mathbf{p}_{m}^{3D} - \mathbf{q}_{j,t}^{3D}\right\|_{2} + n_{r,m,t}^{j}, \tag{14}$$

where $r_{m,t}^{j} = \left\|\mathbf{p}_{m}^{3D} - \mathbf{q}_{j,t}^{3D}\right\|_{2}$ denotes the true distance; $n_{r,m,t}^{j} \sim \mathcal{N}\left(0, \sigma_{r}^{2}\right)$ is the measurement error, and σ_{r}^{2} is its variance.

Denote the N_A^U UAV-As ($N_A^U \geq 3$) serving the m-th UE as the set $\mathcal{N}_A^{U_m}$ ($\mathcal{N}_A^{U_m} \in \mathcal{N}_A$), then the distance measurements available to the UE form the following vector:

$$\hat{\mathbf{r}}_{m,t} = \left[\cdots, \hat{r}_{m,t}^{j}, \cdots\right]^{T} = \mathbf{r}_{m,t} + \mathbf{n}_{\mathbf{r},m,t}, \quad j \in \mathcal{N}_A^{U_m}, \tag{15}$$

where $\mathbf{r}_{m,t} = \left[\cdots, r_{m,t}^{j}, \cdots\right]^{T}$ ($j \in \mathcal{N}_A^{U_m}$); $\mathbf{n}_{\mathbf{r},m,t} = \left[\cdots, n_{r,m,t}^{j}, \cdots\right]^{T}$ is the noise vector consisting of N_A^U i.i.d. measurement errors, and its covariance matrix can be written as $\mathbf{R}_{\mathbf{r}} = \sigma_{r}^{2} \cdot \mathbf{I}_{N_A^U}$.

In practice, the true locations of UAV-As are time-varying and unavailable to UEs. Thus, UEs can only use UAV-As' HPs and the following measurement equations for position estimation:

$$\bar{\mathbf{r}}_{m}\left(\mathbf{p}_{m}\right) = \left[\cdots, \bar{r}_{m}^{j}\left(\mathbf{p}_{m}\right), \cdots\right]^{T} = \left[\cdots, \left\|\mathbf{p}_{m}^{3D} - \mathbf{q}_{j}^{\circ,3D}\right\|_{2}, \cdots\right]^{T}. \tag{16}$$

The iterative least-squares (ILS) method that estimates unknown parameters in an iterative manner through Taylor-series linearization is used to determine UEs' locations [34]. Denote the m-th UE's location estimate obtained in the l-th iteration of ILS as $\hat{\mathbf{p}}_{m,t}^{(l)} \in \mathbb{R}^{2\times 1}$ ($\hat{\mathbf{p}}_{m,t}^{(l),3D} = \left[\left(\hat{\mathbf{p}}_{m,t}^{(l)}\right)^T, 0\right]^T$), then the first-order Taylor-series expansion of $\bar{\mathbf{r}}_m\left(\mathbf{p}_m\right)$ at $\hat{\mathbf{p}}_{m,t}^{(l)}$ can be written as

$$\bar{\mathbf{r}}_m\left(\mathbf{p}_m\right) \simeq \bar{\mathbf{r}}_m\left(\hat{\mathbf{p}}_{m,t}^{(l)}\right) + \mathbf{H}_m\left(\hat{\mathbf{p}}_{m,t}^{(l)}\right)\left(\mathbf{p}_m - \hat{\mathbf{p}}_{m,t}^{(l)}\right), \tag{17}$$

where

$$\mathbf{H}_m\left(\hat{\mathbf{p}}_{m,t}^{(l)}\right) = \left.\frac{\partial \bar{\mathbf{r}}_m\left(\mathbf{p}_m\right)}{\partial \mathbf{p}_m}\right|_{\hat{\mathbf{p}}_{m,t}^{(l)}} = \left[\cdots, \mathbf{h}_m^j\left(\hat{\mathbf{p}}_{m,t}^{(l)}\right), \cdots\right]^T = \left[\cdots, \frac{\left(\hat{\mathbf{p}}_{m,t}^{(l)} - \mathbf{q}_j^{\circ}\right)}{\left\|\hat{\mathbf{p}}_{m,t}^{(l),3D} - \mathbf{q}_j^{\circ,3D}\right\|_2}, \cdots\right]^T \tag{18}$$

is the Jacobian matrix of equation (16) at $\hat{\mathbf{p}}_{m,t}^{(l)}$.

Then, the LS estimate of the UE's location obtained in the $(l+1)$-th iteration is given by

$$\hat{\mathbf{p}}_{m,t}^{(l+1)} = \hat{\mathbf{p}}_{m,t}^{(l)} + \mathbf{S}\left(\hat{\mathbf{p}}_{m,t}^{(l)}\right)\left[\hat{\mathbf{r}}_{m,t} - \bar{\mathbf{r}}_m\left(\hat{\mathbf{p}}_{m,t}^{(l)}\right)\right], \tag{19}$$

where

$$\mathbf{S}\left(\hat{\mathbf{p}}_{m,t}^{(l)}\right) = \mathbf{P}\left(\hat{\mathbf{p}}_{m,t}^{(l)}\right)\mathbf{H}\left(\hat{\mathbf{p}}_{m,t}^{(l)}\right)^T, \tag{20}$$

$$\mathbf{P}\left(\hat{\mathbf{p}}_{m,t}^{(l)}\right) = \left[\mathbf{H}\left(\hat{\mathbf{p}}_{m,t}^{(l)}\right)^T \mathbf{H}\left(\hat{\mathbf{p}}_{m,t}^{(l)}\right)\right]^{-1}. \tag{21}$$

The estimation result of the UE's location can be obtained after the above iteration converges.

III. Performance Analysis and Problem Formulation

The proposed SCC co-design scheme takes into account the UAV position uncertainty caused by sensing and control errors, which has often been overlooked in previous research. Due to this additional consideration, existing analysis methods and performance metrics are unsuitable for the considered system. Therefore, in the first two subsections of this section, we first analyze the stability of UAV-As in two operation modes, and then derive the mean-square error (MSE) of UE positioning in the presence of UAV position uncertainty. It is found that the scheduling of UAV-A state sensing and the blocklength for the transmission of sensing data are two key factors affecting the position accuracy. Then, at the end of this section, we formulate the sensing scheduling and blocklength allocation for reducing the resource consumption of positioning services as a QoS-constrained optimization problem, which will be solved using the algorithm presented in the next section.

A. UAV Stability Prediction in Different Operation Modes

The aim of this subsection is to predict the stability of each UAV-A in the next time slot $(t+1)$ before the CC generates the scheduling commands for the current time slot (t). The UAV-A's dynamics model in two operation modes has been derived in Section II.B. However, it is noteworthy that the dynamics model shown in equation (12) uses the true state of UAV-A ($\mathbf{x}_{j,t}$) when calculating its future state, which is unknown in practice. Therefore, in order to predict the UAV-A's state in time slot $t+1$, we need to replace $\mathbf{x}_{j,t}$ in equation (12) with other variables whose values or distributions are available to the CC. We assume that the last successful state sensing was performed Δt_j^c time slots ago. Then, according to equations (11) and (12), the expression for $\mathbf{x}_{j,t}$ can be written as

$$\mathbf{x}_{j,t} = (\mathbf{A}_j + \mathbf{B}_j\mathbf{K}_j)^{\Delta t_j^c}\mathbf{x}_{j,t-\Delta t_j^c} + \left[\sum_{k=0}^{\Delta t_j^c-1} \mathbf{A}_j^k\mathbf{B}_j\mathbf{K}_j(\mathbf{A}_j + \mathbf{B}_j\mathbf{K}_j)^{\Delta t_j^c-k-1}\right]\boldsymbol{\eta}_{j,t-\Delta t_j^c} + \sum_{k=0}^{\Delta t_j^c-1}\mathbf{A}_j^k\mathbf{w}_{j,t-k-1}. \quad (22)$$

Moreover, utilizing the relationship $\mathbf{x}_{j,t-\Delta t_j^c} = \hat{\mathbf{x}}_{j,t-\Delta t_j^c} - \boldsymbol{\eta}_{j,t-\Delta t_j^c}$ and equation (11), the above equation can be further rewritten as

$$\mathbf{x}_{j,t} = \bar{\mathbf{x}}_{j,t}^{(\Delta t_j^c)} + \left[\left(\sum_{k=0}^{\Delta t_j^c-1} \mathbf{A}_j^k\mathbf{B}_j\mathbf{K}_j(\mathbf{A}_j + \mathbf{B}_j\mathbf{K}_j)^{\Delta t_j^c-k-1}\right) - (\mathbf{A}_j + \mathbf{B}_j\mathbf{K}_j)^{\Delta t_j^c}\right]\boldsymbol{\eta}_{j,t-\Delta t_j^c} + \sum_{k=0}^{\Delta t_j^c-1}\mathbf{A}_j^k\mathbf{w}_{j,t-k-1}. \quad (23)$$

Substituting this equation into equation (12), the UAV-A's dynamics model can be rewritten as

$$\begin{aligned}
\mathbf{x}_{j,t+1}^{(c)} &= \mathbf{A}_j^{(c)}\bar{\mathbf{x}}_{j,t}^{(\Delta t_j^c)} + \left(\mathbf{A}_j^{(c)}\mathbf{C}_j^{(\Delta t_j^c)}\boldsymbol{\eta}_{j,t-\Delta t_j^c} + \mathbf{B}_j\mathbf{K}_j\boldsymbol{\eta}_{j,t}\right) + \left(\sum_{k=0}^{\Delta t_j^c-1}\mathbf{A}_j^{(c)}\mathbf{A}_j^k\mathbf{w}_{j,t-k-1} + \mathbf{w}_{j,t}\right), \text{closed-loop},\\
\mathbf{x}_{j,t+1}^{(o)} &= \mathbf{A}_j^{(c)}\bar{\mathbf{x}}_{j,t}^{(\Delta t_j^c)} + \mathbf{A}_j\mathbf{C}_j^{(\Delta t_j^c)}\boldsymbol{\eta}_{j,t-\Delta t_j^c} + \sum_{k=0}^{\Delta t_j^c}\mathbf{A}_j^k\mathbf{w}_{j,t-k}, \qquad \text{open-loop},
\end{aligned} \quad (24)$$

where

$$\mathbf{A}_j^{(c)} = \mathbf{A}_j + \mathbf{B}_j\mathbf{K}_j \quad (25)$$

is the closed loop state matrix, and

$$\mathbf{C}_j^{(\Delta t_j^c)} = \left[\sum_{k=0}^{\Delta t_j^c-1}\mathbf{A}_j^k\mathbf{B}_j\mathbf{K}_j\left(\mathbf{A}_j^{(c)}\right)^{\Delta t_j^c-k-1} - \left(\mathbf{A}_j^{(c)}\right)^{\Delta t_j^c}\right]. \quad (26)$$

Then, the covariance matrix of the UAV-A's state in time slot $t+1$ can be expressed as

$$\begin{aligned}
\mathbf{Q}_{\mathbf{x},j,t+1}^{(c)} = E\left\{\left(\mathbf{x}_{j,t+1}^{(c)}\right)\left(\mathbf{x}_{j,t+1}^{(c)}\right)^T\right\} &= \left(\mathbf{A}_j^{(c)}\bar{\mathbf{x}}_{j,t}^{(\Delta t_j^c)}\right)\left(\mathbf{A}_j^{(c)}\bar{\mathbf{x}}_{j,t}^{(\Delta t_j^c)}\right)^T + \left(\mathbf{A}_j^{(c)}\mathbf{C}_j^{(\Delta t_j^c)}\right)\mathbf{R}_{\boldsymbol{\eta},j}\left(\mathbf{A}_j^{(c)}\mathbf{C}_j^{(\Delta t_j^c)}\right)^T\\
&\quad + (\mathbf{B}_j\mathbf{K}_j)\mathbf{R}_{\boldsymbol{\eta},j}(\mathbf{B}_j\mathbf{K}_j)^T + \sum_{k=0}^{\Delta t_j^c-1}\left(\mathbf{A}_j^{(c)}\mathbf{A}_j^k\right)\mathbf{Q}_{\mathbf{w}}\left(\mathbf{A}_j^{(c)}\mathbf{A}_j^k\right)^T + \mathbf{Q}_{\mathbf{w}},
\end{aligned} \quad (27)$$

$$\mathbf{Q}_{\mathbf{x},j,t+1}^{(o)} = E\left\{\left(\mathbf{x}_{j,t+1}^{(o)}\right)\left(\mathbf{x}_{j,t+1}^{(o)}\right)^T\right\} = \left(\mathbf{A}_j^{(\phi)}\bar{\mathbf{x}}_{j,t}^{\left(\Delta t_j^c\right)}\right)\left(\mathbf{A}_j^{(\phi)}\bar{\mathbf{x}}_{j,t}^{\left(\Delta t_j^c\right)}\right)^T + \left(\mathbf{A}_j\mathbf{C}_j^{\left(\Delta t_j^c\right)}\right)\mathbf{R}_{\boldsymbol{\eta},j}\left(\mathbf{A}_j\mathbf{C}_j^{\left(\Delta t_j^c\right)}\right)^T + \sum_{k=0}^{\Delta t_j^c}\left(\mathbf{A}_j^k\right)\mathbf{Q}_{\mathbf{w}}\left(\mathbf{A}_j^k\right)^T. \tag{28}$$

We mainly focus on the UAV position uncertainty, whose covariance matrix can be written as

$$\mathbf{Q}_{\Delta\mathbf{q},j,t+1}^{(c)} = \left(\mathbf{Q}_{\mathbf{x},j,t+1}^{(c)}\right)_{2\times 2}, \text{ closed-loop;} \qquad \mathbf{Q}_{\Delta\mathbf{q},j,t+1}^{(o)} = \left(\mathbf{Q}_{\mathbf{x},j,t+1}^{(o)}\right)_{2\times 2}, \text{ open-loop.} \tag{29}$$

B. UE Positioning Performance with UAV Control Error

In this subsection, we further analyze the performance of positioning services in the presence of UAV control error. According to the model described in Section II.C, the estimation error of the m-th UE's location in the $(l+1)$-th iteration of ILS can be expressed as

$$\Delta\mathbf{p}_{m,t+1}^{(l+1)} = \hat{\mathbf{p}}_{m,t+1}^{(l+1)} - \mathbf{p}_m = \left(\hat{\mathbf{p}}_{m,t+1}^{(l)} - \mathbf{p}_m\right) + \mathbf{S}\left(\hat{\mathbf{p}}_{m,t+1}^{(l)}\right)\left[\hat{\mathbf{r}}_{m,t+1} - \bar{\mathbf{r}}_m\left(\hat{\mathbf{p}}_{m,t+1}^{(l)}\right)\right]. \tag{30}$$

With an appropriate UAV control strategy and good initial guesses, the location estimate will be close to the true location ($\mathbf{p}_m$) after several iterations [21]. Thus, by replacing $\hat{\mathbf{p}}_{m,t+1}^{(l)}$ in the above equation with $\mathbf{p}_m$, the estimation error after convergence can be written as

$$\Delta\mathbf{p}_{m,t+1} = \hat{\mathbf{p}}_{m,t+1} - \mathbf{p}_m = \mathbf{S}\left(\mathbf{p}_m\right)\left[\hat{\mathbf{r}}_{m,t+1} - \bar{\mathbf{r}}_m\left(\mathbf{p}_m\right)\right]. \tag{31}$$

The matrix $\mathbf{S}\left(\mathbf{p}_m\right)$ can be calculated using equation (20). We then derive the expression for term $[\hat{\mathbf{r}}_{m,t+1} - \bar{\mathbf{r}}_m\left(\mathbf{p}_m\right)]$. Applying the first-order Taylor-series expansion to equation (14) based on the relationship $\mathbf{q}_{j,t+1} = \mathbf{q}_j^{\circ} + \Delta\mathbf{q}_{j,t+1}$ ($\mathbf{q}_{j,t+1}^{3D} = \mathbf{q}_j^{\circ,3D} + \left[\Delta\mathbf{q}_{j,t+1}^T, 0\right]^T$), $\hat{r}_{m,t+1}^j$ can be approximated as

$$\hat{r}_{m,t+1}^j \simeq \left\|\mathbf{p}_m^{3D} - \mathbf{q}_j^{\circ,3D}\right\|_2 - \mathbf{h}_m^j(\mathbf{p}_m)^T\Delta\mathbf{q}_{j,t+1} + n_{r,m,t+1}^j = \bar{r}_m^j\left(\mathbf{p}_m\right) - \mathbf{h}_m^j(\mathbf{p}_m)^T\Delta\mathbf{q}_{j,t+1} + n_{r,m,t+1}^j. \tag{32}$$

Then, term $[\hat{\mathbf{r}}_{m,t+1} - \bar{\mathbf{r}}_m\left(\mathbf{p}_m\right)]$ can be rewritten as

$$\hat{\mathbf{r}}_{m,t+1} - \bar{\mathbf{r}}_m\left(\mathbf{p}_m\right) = -\left[\cdots, \mathbf{h}_m^j(\mathbf{p}_m)^T\Delta\mathbf{q}_{j,t+1}, \cdots\right]^T + \left[\cdots, n_{r,m,t+1}^j, \cdots\right]^T = -\boldsymbol{\beta}_{m,t+1} + \mathbf{n}_{\mathbf{r},m,t+1}. \tag{33}$$

where $\boldsymbol{\beta}_{m,t+1} = \left[\cdots, \mathbf{h}_m^j(\mathbf{p}_m)^T\Delta\mathbf{q}_{j,t+1}, \cdots\right]^T$.

Substituting the above equation into equation (31), the covariance matrix of the m-th UE's position error in time slot $t+1$ can be expressed as

$$\begin{aligned}\mathbf{Q}_{\Delta\mathbf{p},m,t+1}^{(\boldsymbol{\xi}_{m,t})} &= E\left\{\Delta\mathbf{p}_{m,t+1}\Delta\mathbf{p}_{m,t+1}^T\right\} = E\left\{\mathbf{S}(\mathbf{p}_m)\left(-\boldsymbol{\beta}_{m,t+1} + \mathbf{n}_{\mathbf{r},m,t+1}\right)\left(-\boldsymbol{\beta}_{m,t+1} + \mathbf{n}_{\mathbf{r},m,t+1}\right)^T\mathbf{S}(\mathbf{p}_m)^T\right\} \\ &= \mathbf{S}(\mathbf{p}_m)\left[E\left\{\boldsymbol{\beta}_{m,t+1}\boldsymbol{\beta}_{m,t+1}^T\right\} + E\left\{\mathbf{n}_{\mathbf{r},m,t+1}\mathbf{n}_{\mathbf{r},m,t+1}^T\right\}\right]\mathbf{S}(\mathbf{p}_m)^T \\ &= \sigma_r^2\mathbf{P}(\mathbf{p}_m) + \mathbf{S}(\mathbf{p}_m)\,\mathrm{diag}\left(\ldots, \mathbf{h}_m^j(\mathbf{p}_m)^T\mathbf{Q}_{\Delta\mathbf{q},j,t+1}^{(\xi_{m,j,t})}\mathbf{h}_m^j\left(\mathbf{p}_m\right), \ldots\right)\mathbf{S}(\mathbf{p}_m)^T,\end{aligned} \tag{34}$$

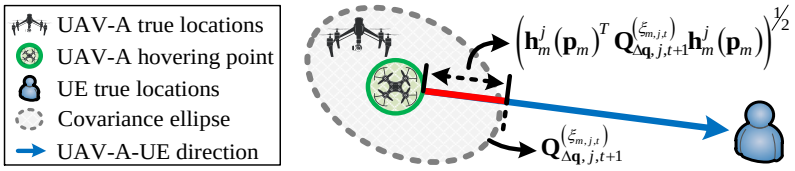

Fig. 2. Explanation of UAV control errors' impact on UE positioning.

where the vector $\boldsymbol{\xi}_{m,t} = [\cdots, \xi_{m,j,t}, \cdots]^T$ $(j \in \mathcal{N}_A^{U_m})$ represents the operation modes of the N_A^U UAV-As serving the m-th UE; $\xi_{m,j,t}$ could be either c or o, indicating the operation mode of the j-th UAV-A in time slot t; the matrix $\mathbf{Q}_{\Delta\mathbf{q},j,t+1}^{(\xi_{m,j,t})}$ can be calculated using equation (29).

As can be seen from equation (34), the covariance matrix of the UE position error can be written as the sum of two terms. The first term $\sigma_r^2 \mathbf{P}(\mathbf{p}_m)$ denotes the position error caused by distance measurement errors, reflecting the position accuracy in the absence of UAV position uncertainty. The second term $\mathbf{S}(\mathbf{p}_m)\,\mathrm{diag}\left(\ldots, \mathbf{h}_m^j(\mathbf{p}_m)^T \mathbf{Q}_{\Delta\mathbf{q},j,t+1}^{(\xi_{m,j,t})} \mathbf{h}_m^j(\mathbf{p}_m), \ldots\right) \mathbf{S}(\mathbf{p}_m)^T$ indicates the performance degradation of positioning services caused by UAV control errors. Fig. 2 gives an intuitive explanation of UAV control errors' impact on UE positioning. According to equation (24), UAV control error can be represented as a linear combination of a set of independent Gaussian random variables. Thus, the control error also follows a Gaussian distribution and its covariance matrix ($\mathbf{Q}_{\Delta\mathbf{q},j,t+1}^{(\xi_{m,j,t})}$) can be visually represented by the gray ellipse in Fig. 2. Then, the term $\mathbf{h}_m^j(\mathbf{p}_m)^T \mathbf{Q}_{\Delta\mathbf{q},j,t+1}^{(\xi_{m,j,t})} \mathbf{h}_m^j(\mathbf{p}_m)$ in equation (34) can be intuitively understood as the square of the projected length of the j-th UAV-A's covariance ellipse in the UAV-A-UE direction. Finally, the matrix $\mathbf{S}(\mathbf{p}_m)$ is used to convert the term $\mathbf{h}_m^j(\mathbf{p}_m)^T \mathbf{Q}_{\Delta\mathbf{q},j,t+1}^{(\xi_{m,j,t})} \mathbf{h}_m^j(\mathbf{p}_m)$ into its contribution to the covariance matrix of UE position error through a linear transformation.

Then, according to equation (34), the MSE of UE positioning in the presence of UAV control error can be expressed as

$$MSE_{m,t+1}^{(\boldsymbol{\xi}_{m,t})} = \mathrm{tr}\left(\mathbf{Q}_{\Delta\mathbf{p},m,t+1}^{(\boldsymbol{\xi}_{m,t})}\right). \tag{35}$$

C. QoS-Constrained Optimization Problem

According to the analysis results described above, the position accuracy of the considered system is affected mainly by the UAV control error in the next time slot $(t+1)$. The UAV control error itself mainly depends on UAV-As' operation modes in the current time slot (t). Obviously, the schedule of the UAV-A state sensing is one of the determinant factors of operation

modes. In this paper, we use a binary vector $\boldsymbol{\varphi}_t = [\cdots, \varphi_{j,t}, \cdots] \in \mathbb{Z}^{1\times N_A}$ to indicate the sensing schedule. $\varphi_{j,t} = 1$ means that the j-th UAV-A is required to perform state sensing in time slot t, while $\varphi_{j,t} = 0$ means the opposite. If a UAV-A is not scheduled in the current time slot, it will of course be controlled in OL mode. However, it is noteworthy that $\varphi_{j,t} = 1$ is just a necessary condition for CL mode. The implementation of CL mode also requires the successful transmission of sensing data.

We use variable $\theta^i_{j,t}$ to represent the blocklength allocated for the transmission of sensing data corresponding to the j-th UAV-A and i-th UAV-B; vector $\boldsymbol{\theta}_{j,t} = \left[\cdots, \theta^i_{j,t}, \cdots\right] \in \mathbb{R}^{1\times 3}$ ($i \in \mathcal{N}_B^{A_j}$) denotes the blocklength for the transmission of the j-th UAV-A's sensing data. Then, the success rate of the data transmission corresponding to the j-th UAV-A and i-th UAV-B can be calculated with equations introduced in Appendix B and denoted as $P^{i,(s)}_{j,t}\left(\theta^i_{j,t}\right)$. In this paper, each UAV-A is assigned three UAV-Bs for state sensing, which is the minimum number required for location estimation. Thus, the probabilities of the two operation modes can be expressed as

$$\begin{aligned} P^{(c)}_{j,t}\left(\varphi_{j,t}, \boldsymbol{\theta}_{j,t}\right) &= \varphi_{j,t} \cdot \prod_{i\in\mathcal{N}_B^{A_j}} P^{i,(s)}_{j,t}\left(\theta^i_{j,t}\right), \quad \text{closed-loop}, \\ P^{(o)}_{j,t}\left(\varphi_{j,t}, \boldsymbol{\theta}_{j,t}\right) &= 1 - P^{(c)}_{j,t}\left(\varphi_{j,t}, \theta_{j,t}\right), \quad \text{open-loop}. \end{aligned} \tag{36}$$

Since each UAV-A has two operation modes, the vector $\boldsymbol{\xi}_{m,t}$ introduced in subsection B has $G = 2^{N_A^U}$ possible values, indicating different "sensing events". The G possible events are represented by the set $\mathcal{G} = \{1, \cdots, G\}$, and the value of $\boldsymbol{\xi}_{m,t}$ in the g-th event ($g \in \mathcal{G}$) is denoted as $\boldsymbol{\xi}^g_{m,t}$. The sets $\mathcal{C}^g_{m,t}$ and $\mathcal{O}^g_{m,t}$ denote the UAV-As operating in CL and OL modes in the g-th event, respectively. Then, the expectation of the MSE of the m-th UE's position estimate is given by

$$MSE_{m,t+1}\left(\boldsymbol{\varphi}_t, \boldsymbol{\theta}_t\right) = \sum_{g\in\mathcal{G}} \left(MSE^{\left(\boldsymbol{\xi}^g_{m,t}\right)}_{m,t+1} \cdot P^{\left(\boldsymbol{\xi}^g_{m,t}\right)}_{m,t}\left(\boldsymbol{\varphi}_t, \boldsymbol{\theta}_t\right) \right), \tag{37}$$

where

$$P^{\left(\boldsymbol{\xi}^g_{m,t}\right)}_{m,t}\left(\boldsymbol{\varphi}_t, \boldsymbol{\theta}_t\right) = \prod_{j\in\mathcal{C}^g_{m,t}} P^{(c)}_{j,t}\left(\varphi_{j,t}, \boldsymbol{\theta}_{j,t}\right) \prod_{j\in\mathcal{O}^g_{m,t}} P^{(o)}_{j,t}\left(\varphi_{j,t}, \boldsymbol{\theta}_{j,t}\right) \tag{38}$$

is the probability of the g-th sensing event; $\boldsymbol{\theta}_t = [\cdots, \boldsymbol{\theta}_{j,t}, \cdots] \in \mathbb{R}^{1\times(3N_A)}$ ($j \in \mathcal{N}_A$). In the following, $MSE_{m,t+1}\left(\boldsymbol{\varphi}_t, \boldsymbol{\theta}_t\right)$ will be used as the performance metric for positioning services.

We hope to reduce the resource consumption of UAV-A state sensing by optimizing the sensing scheduling and blocklength allocation, while ensuring that the position accuracy meets the UEs'

Algorithm 1 Proposed Heuristic Algorithm for Problem (P1)

Input: MSE_m^{Req}, $\mathbf{h}_m^j(\mathbf{p}_m)$ and $\mathbf{P}(\mathbf{p}_m)$ corresponding to each UE; $\mathbf{Q}_{\Delta\mathbf{q},j,t+1}^{(c)}$ and $\mathbf{Q}_{\Delta\mathbf{q},j,t+1}^{(o)}$ corresponding to each UAV-A;

Initialization: Calculate $\sigma_{\Delta\mathbf{q},m}^2$ for each UE according to MSE_m^{Req} and $\mathbf{P}(\mathbf{p}_m)$; (45), (47);

1: *Decoupling of UAV Control:* Formulate problem (P2) for each UAV-A based on $\mathbf{h}_m^j(\mathbf{p}_m)$, $\mathbf{Q}_{\Delta\mathbf{q},j,t+1}^{(c)}$, $\mathbf{Q}_{\Delta\mathbf{q},j,t+1}^{(o)}$ and the method presented in Subsection A; (48)-(49);

2: **for** $j = 1$ to N_A **do**

3: *Sensing Scheduling:* Determine whether the j-th UAV-A needs state sensing according to the strategy described in Subsection B; (51)-(52);

4: *Blocklength Allocation:* Calculate the blocklength for the transmission of the j-th UAV-A's sensing data based on the strategy described in Subsection C; (53);

5: **end for**

Output: $\boldsymbol{\varphi}_t$ indicating the sensing schedule, $\boldsymbol{\theta}_t$ representing the allocated blocklengths.

requirements. This goal could be approached by minimizing the total number of symbols used in each time slot, which can be formulated as the following QoS-constrained optimization problem:

$$(\mathrm{P1}): \quad \min_{\boldsymbol{\varphi}_t, \boldsymbol{\theta}_t} \sum_{j\in\mathcal{N}_A} \sum_{i\in\mathcal{N}_B^{A_j}} \theta_{j,t}^i \tag{39}$$

$$\text{s.t.} \quad MSE_{m,t+1}(\boldsymbol{\varphi}_t, \boldsymbol{\theta}_t) \le MSE_m^{Req}, \qquad \forall m \in \mathcal{M},\, t, \tag{40}$$

where term $\sum_{j\in\mathcal{N}_A} \sum_{i\in\mathcal{N}_B^{A_j}} \theta_{j,t}^i$ denotes the overall blocklength in time slot t; $\boldsymbol{\varphi}_t$ is a binary vector indicating the sensing schedule of UAV-As, while $\boldsymbol{\theta}_t$ is a real vector consisting of the blocklength allocated to each UAV-B for transmitting UAV-As' sensing data; MSE_m^{Req} is the m-th UE's requirement on the MSE of positioning services.

IV. Heuristic Algorithm for Sensing Scheduling and Blocklength Allocation

Due to the binary vector $\boldsymbol{\theta}_t$ as well as the nonlinear constraint (40), problem (P1) is a mixed-integer nonlinear optimization problem, which is difficult to solve, especially when the number of UAV-As is large. Moreover, in the considered system, each UE is served by multiple UAV-As, and each UAV-A could also serve multiple UEs. The coupling among different UAV-As and UEs increases the difficulty of the problem. Therefore, in this section, we develop a heuristic

algorithm to solve this problem efficiently and find a solution that may not be optimal but has satisfactory performance. The most notable advantage of the proposed algorithm is that it decouples the control of each UAV-A, making it suitable for large-scale UAV systems. Algorithm 1 summarizes the overall algorithm, which includes three basic processing steps: "decoupling of UAV control", "sensing scheduling" and "blocklength allocation". The rest of this section presents the principles and implementation details of these three steps.

A. Decoupling of UAV Control

Substituting equations (34) and (35) into (37), the expression of $MSE_{m,t+1}\left(\boldsymbol{\varphi}_t, \boldsymbol{\theta}_t\right)$ can be rewritten as

$$MSE_{m,t+1}\left(\boldsymbol{\varphi}_t, \boldsymbol{\theta}_t\right) = \sigma_r^2 \mathrm{tr}\left(\mathbf{P}\left(\mathbf{p}_m\right)\right) + \mathrm{tr}\left(\mathbf{S}\left(\mathbf{p}_m\right) \bar{\mathbf{D}}_{\Delta\mathbf{q},m,t+1} \mathbf{S}(\mathbf{p}_m)^T\right), \tag{41}$$

where

$$\bar{\mathbf{D}}_{\Delta\mathbf{q},m,t+1}\left(\boldsymbol{\varphi}_t, \boldsymbol{\theta}_t\right) = \sum_{g \in \mathcal{G}} \left(\mathbf{D}_{\Delta\mathbf{q},m,t+1}^{\left(\boldsymbol{\xi}_{m,t}^g\right)} \cdot P_{m,t}^{\left(\boldsymbol{\xi}_{m,t}^g\right)}\left(\boldsymbol{\varphi}_t, \boldsymbol{\theta}_t\right) \right), \tag{42}$$

$$\mathbf{D}_{\Delta\mathbf{q},m,t+1}^{\left(\boldsymbol{\xi}_m^g\right)} = \mathrm{diag}\left(\ldots, \mathbf{h}_m^j(\mathbf{p}_m)^T \mathbf{Q}_{\Delta\mathbf{q},j,t+1}^{\left(\xi_{m,j,t}^g\right)} \mathbf{h}_m^j\left(\mathbf{p}_m\right), \ldots \right). \tag{43}$$

Then, the QoS constraint (40) can be rewritten as

$$\mathrm{tr}\left(\mathbf{S}\left(\mathbf{p}_m\right) \bar{\mathbf{D}}_{\Delta\mathbf{q},m,t+1}\left(\boldsymbol{\varphi}_t, \boldsymbol{\theta}_t\right) \mathbf{S}(\mathbf{p}_m)^T\right) \leq T_m, \tag{44}$$

where

$$T_m = MSE_m^{Req} - \sigma_r^2 \mathrm{tr}\left(\mathbf{P}\left(\mathbf{p}_m\right)\right). \tag{45}$$

Please note that matrix $\bar{\mathbf{D}}_{\Delta\mathbf{q},m,t+1}\left(\boldsymbol{\varphi}_t, \boldsymbol{\theta}_t\right)$ is a diagonal matrix whose diagonal elements denote the expectation of the squared projected length of each UAV-A's covariance ellipse in the UAV-A-UE direction. As can be seen from equation (44), the QoS constraint in problem (P1) only restricts the value obtained through the linear combination of squared projected lengths corresponding to N_A^U UAV-As serving each UE. The coupling among UAV-As makes it difficult to determine which UAV-A should be controlled in CL mode. Therefore, we have the following proposition to decouple the control of UAV-As.

Proposition 1: Inequality (44) holds for the m-th UE if all of the UAV-As ($\forall j \in \mathcal{N}_A^{U_m}$) serving this UE fulfill the following condition:

$$\mathbf{h}_m^j(\mathbf{p}_m)^T \sum_{g \in \mathcal{G}} \left(\mathbf{Q}_{\Delta\mathbf{q},j,t+1}^{\left(\xi_{m,j,t}^g\right)} \cdot P_{m,t}^{\left(\boldsymbol{\xi}_m^g\right)}\left(\boldsymbol{\varphi}_t, \boldsymbol{\theta}_t\right) \right) \mathbf{h}_m^j\left(\mathbf{p}_m\right) \leq \sigma_{\Delta\mathbf{q},m}^2, \tag{46}$$

where

$$\sigma^2_{\Delta\mathbf{q},m} = T_m / \mathrm{tr}\left(\mathbf{P}\left(\mathbf{p}_m\right)\right). \tag{47}$$

Proof: Please refer to Appendix C. ■

Please note that condition (46) is sufficient but not necessary for inequality (44) to hold. With Proposition 1, the constraint on position accuracy is converted into the requirement on the squared projected length of each UAV-A's covariance ellipse. Then, we could consider each UAV-A individually, and the original problem (P1) can be divided into the following subproblems:

$$(\mathrm{P2}): \min_{\varphi_{j,t},\boldsymbol{\theta}_{j,t}} \sum_{i\in\mathcal{N}_B^{A_j}} \theta^i_{j,t} \tag{48}$$

$$\text{s.t.} \quad \mathbf{h}^j_m(\mathbf{p}_m)^T \Big(P^{(c)}_{j,t}\left(\varphi_{j,t},\boldsymbol{\theta}_{j,t}\right)\mathbf{Q}^{(c)}_{\Delta\mathbf{q},j,t+1} + P^{(o)}_{j,t}\left(\varphi_{j,t},\boldsymbol{\theta}_{j,t}\right)\mathbf{Q}^{(o)}_{\Delta\mathbf{q},j,t+1}\Big)\mathbf{h}^j_m\left(\mathbf{p}_m\right) \le \sigma^2_{\Delta\mathbf{q},m}, \quad \forall m\in\mathcal{M}_j, \tag{49}$$

where $\mathcal{M}_j$ is the set of UEs served by the j-th UAV-A.

Although the number of variables in a single problem has been greatly reduced, problem (P2) is still a complex, mixed-integer, nonlinear problem. Thus, later in this section, we use two strategies to perform the sensing scheduling and blocklength allocation for each UAV-A.

B. Strategy for Sensing Scheduling

The main idea of our strategy for sensing scheduling can be summarized as follows: inequality (49) holds for a UAV-A if its stability in OL mode meets the requirements, that is

$$\mathbf{h}^j_m(\mathbf{p}_m)^T\mathbf{Q}^{(o)}_{\Delta\mathbf{q},j,t+1}\mathbf{h}^j_m\left(\mathbf{p}_m\right) \le \sigma^2_{\Delta\mathbf{q},m}, \quad \forall m\in\mathcal{M}_j. \tag{50}$$

Therefore, we will try to control a UAV-A in CL mode if its predicted stability in OL mode approaches the limit. We use the following variable to indicate the gap between the squared projected lengths of the j-th UAV-A in OL mode and UEs' requirements:

$$\kappa_{j,t} = \max_{m\in\mathcal{M}_j}\left\{\mathbf{h}^j_m(\mathbf{p}_m)^T\mathbf{Q}^{(o)}_{\Delta\mathbf{q},j,t+1}\mathbf{h}^j_m\left(\mathbf{p}_m\right) - \lambda^2\cdot\sigma^2_{\Delta\mathbf{q},m}\right\}, \tag{51}$$

where λ is a scaling factor representing our tolerance for the increase in UAV position uncertainty caused by OL modes. Then, our strategy for sensing scheduling can be expressed as

$$\varphi_{j,t} = \begin{cases} 1, & \text{if } \kappa_{j,t}\ge 0, \\ 0, & \text{otherwise.} \end{cases} \tag{52}$$

C. Strategy for Blocklength Allocation

If a UAV-A is chosen to be controlled in CL mode, we hope that the corresponding state sensing could be carried out with a relatively high success rate, so as to avoid its position uncertainty exceeding the tolerable limit. Since this paper is just a preliminary attempt to introduce the SCC co-design into UAV-enabled positioning, we adopt a simple strategy to allocate the blocklength for data transmission. In our strategy, the success rate of state sensing is set to a fixed value $P_{Req}^{(c)}$, and the transmission of sensing data obtained by different UAV-Bs has the same success rate. Then, the blocklength allocated to the i-th UAV-B ($i \in \mathcal{N}_B^{A_j}$) for transmitting the j-th UAV-A's sensing data can be calculated as

$$\theta_{j,t}^{i} = \theta\left(\left(P_{Req}^{(c)}\right)^{1/3}, \gamma_{i,t}\right) \cdot \varphi_{j,t}, \tag{53}$$

where $\theta(\cdot)$ is the blocklength calculation function, and $\gamma_{i,t}$ denotes the signal-to-noise ratio (SNR) of the i-th UAV-B's signal at the corresponding BS. The expressions of $\theta(\cdot)$ and $\gamma_{i,t}$ are derived in Appendix B.

V. Numerical Results

In this section, we conduct a series of simulation experiments and provide the corresponding numerical results to validate the performance of the proposed scheme. First, the importance of SCC co-design for UAV-enabled positioning and the feasibility of our scheme are verified by an experiment. Then, we compare the proposed co-design scheme with two benchmark schemes, namely the "continuous scheme" and "periodic scheme", to reflect the superiority of our scheme.

Fig. 3 shows the test scenario used for performance evaluation and comparison in this section, which consists of 8 UAV-As ($N_A = 8$), 8 UAV-Bs ($N_B = 8$) and 15 UEs ($M = 15$). The origin of Cartesian coordinates is set at the center of the test scenario. UAV-Bs are uniformly deployed on the circle of radius 2 km centered at the origin, and the distance between each UAV-B and its corresponding BS is 1 km. The horizontal coordinates of the 8 UAV-As' HPs are set to $\mathbf{q}_1^{\circ} = [1000, 0]^T$, $\mathbf{q}_2^{\circ} = [785, 715]^T$, $\mathbf{q}_3^{\circ} = [-980, 724]^T$, $\mathbf{q}_4^{\circ} = [-951, 164]^T$, $\mathbf{q}_5^{\circ} = [-382, 990]^T$, $\mathbf{q}_6^{\circ} = [758, -624]^T$, $\mathbf{q}_7^{\circ} = [-836, -820]^T$ and $\mathbf{q}_8^{\circ} = [172, -977]^T$. UEs are randomly located within a square with center at the coordinate origin and side length of 1 km. When assigning N_A^U UAV-As to each UE, we select the subset of UAV-As with the minimum horizontal dilution of precision (HDOP) [10]. HDOP is a metric widely used in wireless positioning, and its value reflects the influence of the geometry of anchor nodes on the horizontal position accuracy. In

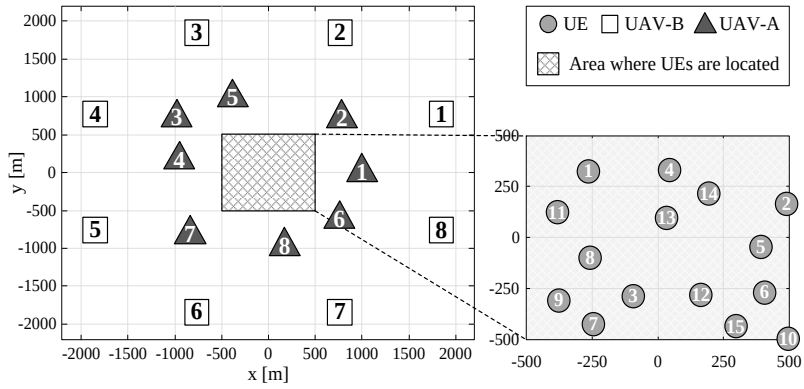

Fig. 3. Test scenario for numerical evaluation.

general, small HDOP values imply satisfactory positioning performance [35]. Thus, the above selection criterion helps to improve the accuracy of positioning services. The same criterion is also used for the selection of the three UAV-Bs responsible for sensing each UAV-A's state.

The key simulation parameters used in this section are summarized as follows: All UAVs in the test scenario, including UAV-As and UAV-Bs, hover at the same altitude $h_v = 50$ m and have the same transmit power $P_t = 30$ dBm; The noise power at terrestrial BSs is $N_0 = -107$ dBm; The number of UAV-As serving each UE is $N_A^U = 3$; The variances of inter-UAV and UAV-A-UE distance measurements are $\sigma_d^2 = 1\ \mathrm{m}^2$ and $\sigma_r^2 = 1\ \mathrm{m}^2$, respectively; UEs have the same requirement on the MSE of positioning services, i.e., $MSE_{Req,m} = 10^2\ \mathrm{m}^2$ ($\forall m \in \mathcal{M}$). The covariance matrices of velocity and acceleration measurements are set to $\mathbf{R_v} = \left(0.5^2\right) \cdot \mathbf{I}_2$ and $\mathbf{R_a} = \left(0.1^2\right) \cdot \mathbf{I}_2$, respectively; The length of each time slot is $\Delta t = 1$ s; The time constant of lag of each UAV-A in responding commanded acceleration is $\rho = 10$ ms; The continuous-time acceleration process noise intensity in x- and y-directions are $\varsigma_x^2 = 0.5^2\ m^2/s^3$ and $\varsigma_y^2 = 0.5^2\ m^2/s^3$, respectively; The feedback gain matrix $\mathbf{K}_j$ for UAV control is generated based on the standard linear quadratic regulator (LQR) control; The scaling factor and success rate in the proposed heuristic algorithm are set to $\lambda = 0.8$ and $P_{Req}^{(c)} = 0.95$, respectively.

A. Feasibility Test of the Proposed Co-Design Scheme

In this subsection, we successively apply two UAV-enabled positioning systems, namely the conventional system without considering state sensing and control as well as the co-design system with the proposed scheme, in the test scenario shown in Fig. 3. The dynamics model of the conventional system is obtained by removing the term $\mathbf{B}_j\mathbf{u}_{j,t}$ from equation (9). The running

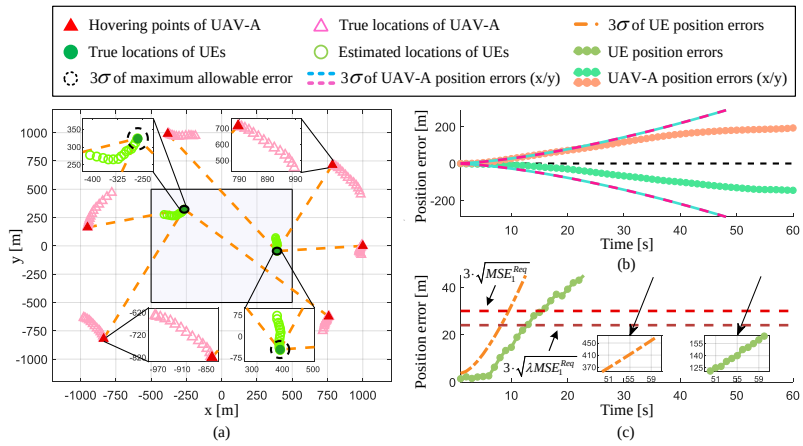

Fig. 4. Test results of the conventional system: Variations of (a) system status, (b) UAV control error (UAV-A 7) and (c) UE positioning performance (UE 1).

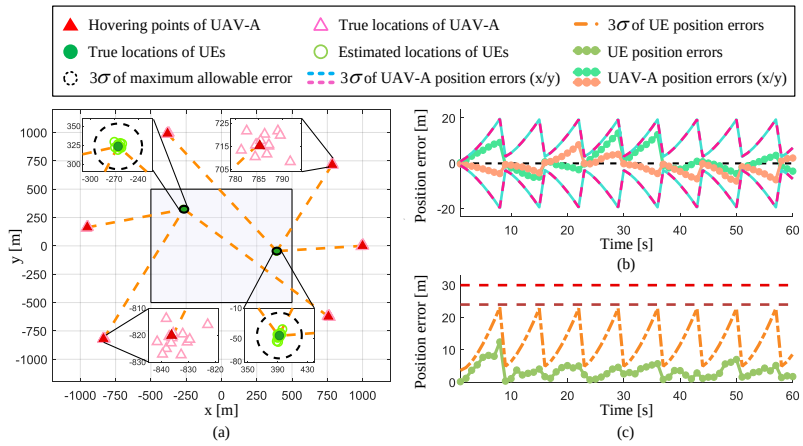

Fig. 5. Test results of the co-design system: Variations of (a) system status, (b) UAV control error (UAV-A 7) and (c) UE positioning performance (UE 1).

time of both systems is 60 time slots (1 min), and the corresponding simulation results are shown in Fig. 4 and Fig. 5. For the simplicity of data presentation, this subsection only presents the simulation results corresponding to a subset of the UAV-As and UEs, which will not reduce the generality of the analysis results.

Fig. 4(a) and Fig. 5(a) show the variations of the two systems' status over time, including the variations of UAV-As' true locations and UEs' location estimates. It can be seen that UAV-As in the conventional system deviate significantly from their HPs. According to Fig. 4(b), these deviations reach hundreds of meters in both x- and y-directions after 40s, which will affect the

system safety. In terms of the position accuracy, as can be seen from Fig. 4(c), the theoretical MSE of the conventional system's positioning services exceeds the 10^2 m^2 required by UEs only 10s after the experiment starts. About 5s later, the position estimation error of ILS also exceeds the tolerable limit. At the end of the experiment, the theoretical MSE and position error of the conventional system have reached large values of 156.7^2 m^2 and 164.2 m, respectively. These phenomena indicate that sensing and control functions are indispensable for the implementation of UAV-enabled positioning.

As shown in Fig. 5(a), during the experiment, UAV-As in the co-design system always stay in the vicinity of their HPs, and the position estimation error of each UE is also kept within an acceptable range. According to Fig. 5(b), the co-design system maintains deviations between the UAV-A's true location and its HP in both x- and y-directions within the range of ± 20.00 m. The variation of UAV control error in Fig. 5(b) can be interpreted as follows: When the position uncertainty of the UAV-A is relatively small, such as time period 1s-7s in this experiment, UAV-A is controlled in OL mode to reduce resource consumption, resulting in an increase in control error. If the UAV position uncertainty approaches the limit defined by inequality (46), the co-design system allocates wireless resources for state sensing to the UAV-A so that it can be controlled in CL mode. Therefore, UAV control errors in the co-design system fluctuate dynamically with time. Moreover, as can be seen from Fig. 5(c), the theoretical MSE of the co-design system's positioning services exhibits a variation similar to the UAV control error. This phenomenon is reasonable because, according to equation (34), position uncertainty for the UAV-As is one of the main factors affecting the performance of UE positioning. It is noteworthy that although the quality of positioning services fluctuates with time, the co-design system can always meet UEs' requirements. During the experiment, the maximum theoretical MSE and position estimation error are 7.717^2 m^2 and 12.44 m, respectively. The above results demonstrate the feasibility of our SCC co-design scheme.

B. The Superiority of Co-Design over the Continuous Scheme

In this subsection, we test and compare the performance of our proposed scheme and the continuous scheme commonly used in existing systems. In the continuous scheme, the state sensing for each UAV-A is performed in each time slot, i.e., $\varphi_{j,t} = 1$ ($\forall j \in \mathcal{N}_A$, $\forall t$). The blocklength in both schemes is determined by the strategy shown in equation (53). Fig. 6 and Fig. 7 show the numerical results obtained in this experiment.

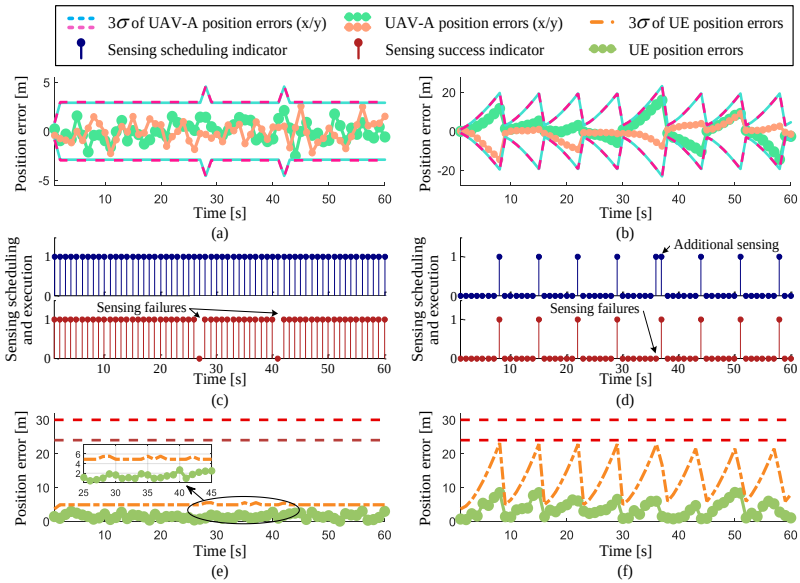

Fig. 6. Performance comparison between the continuous and proposed schemes: UAV control error (UAV-A 7) of the (a) continuous and (b) proposed schemes; Sensing scheduling and execution status (UAV-A 7) of the (c) continuous and (d) proposed schemes; UE positioning performance (UE 1) of the (e) continuous and (f) proposed schemes.

As can be seen from Fig. 6(a) and (b), the UAV control error of the continuous scheme is basically maintained within the range of ± 2.973 m, while that of the proposed scheme is mostly between -19.33 m and 19.33 m. Please note that at 28s and 42s for the operation of the continuous scheme, the envelope of UAV control error expands significantly and reaches ± 4.607 m. According to the sensing scheduling and execution results shown in Fig. 6(c), the major cause of these phenomena is the unexpected OL control due to failed sensing data transmissions at 27s and 41s. As shown in Fig. 6(b) and (d), a similar phenomenon also occurs at 37s for the operation of the proposed scheme. Fortunately, the proposed scheme performs additional state sensing at this time, avoiding a further increase in UAV control error. This result indicates the proposed scheme's adaptability to transmission failures. Although it seems that the continuous scheme has much smaller UAV control errors than the proposed scheme, the data in Fig. 6(e) and (f) show that high control accuracy is unnecessary for positioning services. According to Fig. 6(e), during the experiment, the maximum theoretical MSE and position error of the continuous scheme's positioning services are $1.847^2\ m^2$ and 3.023 m, which are far below the UEs' tolerable limits. In terms of the proposed scheme (Fig. 6(f)), its maximum theoretical MSE and position error are $7.717^2\ m^2$ and 8.537 m, which are much larger than those of the continuous scheme

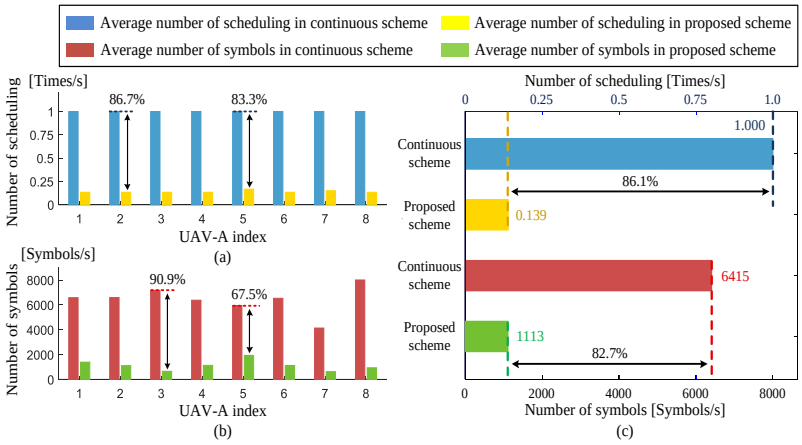

Fig. 7. Performance comparison between the continuous and proposed schemes: Number of (a) scheduling and (b) symbols corresponding to each UAV-A in two schemes; (c) average number of scheduling and symbols among all UAV-As in two schemes.

but still meet the UEs' requirements.

Since both of the schemes tested in this subsection meet UEs' requirements on position accuracy, we turn to compare their resource consumption. The average number of scheduling (times/s) and the average number of symbols (symbols/s) used for data transmission are chosen as the metrics for evaluating the resource efficiency. As can be seen from Fig. 7(a), compared with the continuous scheme, the proposed scheme significantly reduces the average number of scheduling for each UAV-A. The reduction in the number of scheduling is between 83.3% and 86.7%. Moreover, according to Fig. 7(b), the proposed scheme also greatly reduces the number of symbols required for the state sensing of each UAV-A, and the reduction is within the range of $67.5\% \sim 90.9\%$. Fig. 7(c) shows the resource consumption of the two schemes from an overall system perspective. For the overall system, the proposed scheme reduces the number of scheduling and symbols for UAV-A state sensing by 86.1% and 82.7%, respectively.

The above numerical results show that compared with the commonly used continuous scheme, the proposed SCC co-design scheme can schedule and allocate wireless resources adaptively according to the system status, thus improving the resource efficiency of positioning services.

C. The Superiority of Co-Design over the Periodic Scheme

The simulation results presented in the previous two subsections may give the illusion that the state sensing in the proposed scheme is performed periodically. Therefore, in this subsection, we compare our scheme with the periodic scheme to illustrate their differences as well as the

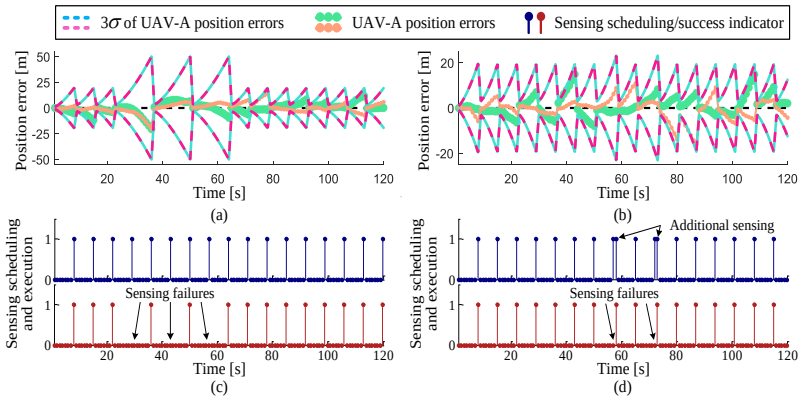

Fig. 8. Performance comparison between the periodic and proposed schemes in the low-success-rate situation: UAV control error (UAV-A 7) of the (a) periodic and (b) proposed schemes; Sensing scheduling and execution status (UAV-A 7) of the (c) periodic and (d) proposed schemes.

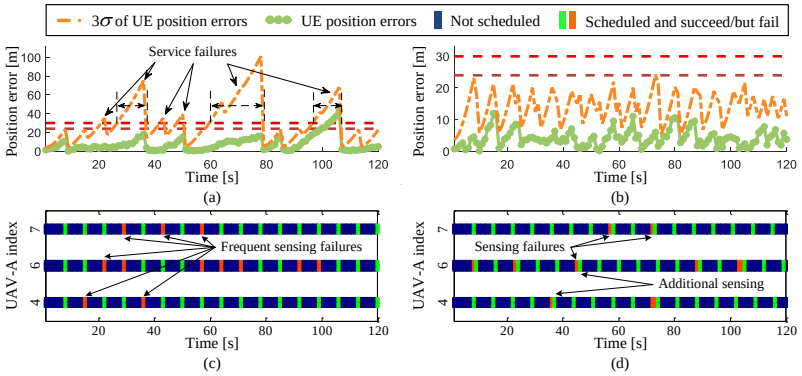

Fig. 9. Performance comparison between the periodic and proposed schemes in the low-success-rate situation: UE positioning performance (UE 1) of the (a) periodic and (b) proposed schemes; Sensing scheduling and execution status (UAV-As 4, 6 and 7 that serve UE 1) of the (c) periodic and (d) proposed schemes.

superiority of the proposed scheme. In the periodic scheme, the state sensing for each UAV-A is performed periodically at a constant time interval, regardless of whether the sensing data is successfully transmitted. For the parameter setting mentioned at the beginning of this section, this time interval is set to 7 time slots (i.e., 7s). We set up two test situations for the comparison of the two schemes, namely the low-success-rate situation and the intermittent-link-blocking situation. In each case, the running time of both schemes is 120 time slots (2 min).

In the low-success-rate situation, the success rate of state sensing ($P_{Req}^{(c)}$) is reduced from 0.95 to 0.70, so as to simulate frequent transmission failures due to limited wireless resources and fading channel conditions. Fig. 8 and Fig. 9 show the performance of the two schemes in this

test situation. As can be seen from Fig. 8(c), at 29s, 43s and 57s of the operation of the periodic scheme, the state sensing for the UAV-A is scheduled but not successfully executed. According to Fig. 8(a), the envelope of UAV control error continues to expand after these moments until state sensing is scheduled and executed successfully in the next "sensing occasion". During the experiment, the size of the envelope of UAV control error in the periodic scheme reaches a maximum of ± 50.05 m. For the proposed scheme, the deviation between the UAV-A's true location and its HP is basically maintained within the range of ± 19.33 m, as shown in Fig. 8(b). Although sensing failures also occur in the proposed scheme (at 57s and 72s in Fig. 8(d)) and lead to temporary expansions of the envelope of UAV control error, these trends are quickly reversed by performing additional state sensing in the next time slots (58s and 73s). The differences in sensing scheduling between the two schemes also affect the quality of their positioning services. As shown in Fig. 9(a), during the experiment, the theoretical MSE of the periodic scheme exceeds the tolerable limit several times, resulting in "service failures". On the contrary, as can be seen from Fig. 9(b), the performance of the proposed scheme's positioning services always meets UEs' requirements. According to Fig. 9(c) and (d), the main reason for these phenomena is that the proposed scheme has the ability to perform additional state sensing according to the system status, making it much more reliable than the periodic scheme in low-success-rate situations.

The term "intermittent-link-blocking" refers to a situation where one or more UAV-As are unable to perform state sensing within a short period of time due to equipment failure or other reasons. In this experiment, we assume that the sensing links for UAV-As 4, 6 and 7 are blocked in the time periods of 63s-72s, 98s-103s and 20s-24s, respectively. Fig. 10 shows the test results of the two schemes in this situation. As can be seen from Fig. 10(a) and (b), service failures occur during the operation of both schemes. However, the number and duration of service failures in the proposed scheme are much smaller than those in the periodic scheme. Moreover, during the experiment, the maximum theoretical MSE of the periodic and proposed schemes is 18.47^2 m^2 and 12.01^2 m^2, respectively. Thus, compared with the periodic scheme, the proposed scheme significantly reduces the impact of link blocking on the quality of positioning services. In Fig. 10(e), the service failure rate of each UE in the experiment is calculated. It can be seen clearly that our scheme greatly reduces the service failure rate of each of the 15 UEs, and the reduction ranges from 76.2% to 96.3%. The data in Fig. 10(c) and (d) illustrate that the proposed scheme's ability to perform additional state sensing is also the major cause of these phenomena.

From the above experimental results, it can be concluded that the proposed SCC co-design

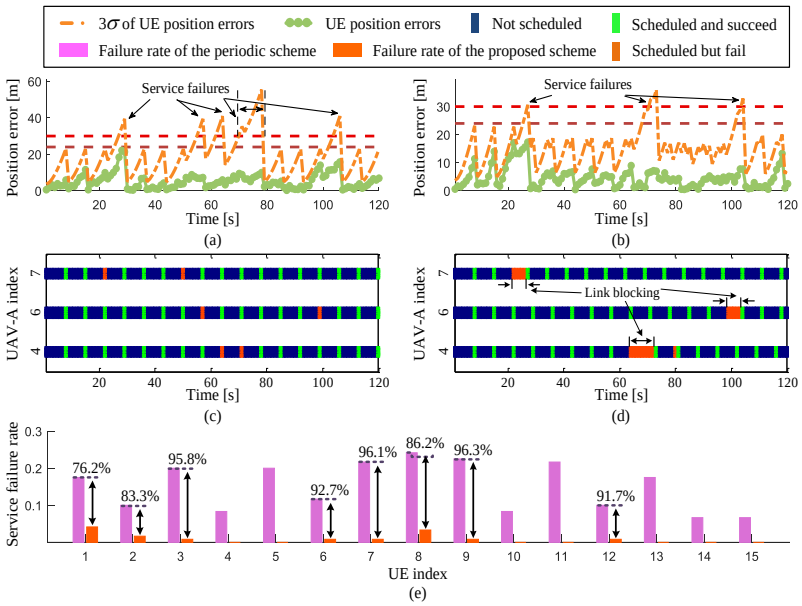

Fig. 10. Performance comparison between the periodic and proposed schemes in the intermittent-link-blocking situation: UE positioning performance (UE 1) of the (a) periodic and (b) proposed schemes; Sensing scheduling and execution status (UAV-As 4, 6 and 7) of the (c) periodic and (d) proposed schemes; (e) Service failure rate corresponding to each UE in two schemes.

scheme can achieve much better service reliability than the periodic scheme in harsh situations.

VI. Conclusion

In this paper, a SCC co-design scheme is proposed for UAV-enabled positioning services that can both meet UEs' requirements and achieve high resource efficiency. Unlike previous research, this paper focuses on the interaction among the sensing, communication and control functions in UAV-enabled positioning systems, especially the UAV position uncertainty caused by sensing and control errors. Specifically, we first establish mathematical models for UAV state sensing and control. Then, a general framework that considers the imperfections of each function is presented to describe the relationship between the design of SCC functions and position accuracy. Based on this framework, we further study the problem of joint sensing scheduling and blocklength allocation for reducing the resource consumption of positioning services, and develop a heuristic algorithm to solve this problem efficiently. Numerical results demonstrate that compared with two benchmark schemes, our proposed scheme improves the service reliability or resource efficiency by more than 75% or 80%, respectively. In future work, we will consider the mobility of UEs

and investigate the real-time tracking service based on the UAV-enabled positioning via SCC co-design.

APPENDIX A
UAV DYNAMICS MODEL

In this paper, we use the following third-order linear model to describe the dynamics of the j-th UAV-A:

$$\Delta\dot{q}_j^{(x)} = v_j^{(x)}, \qquad \Delta\dot{q}_j^{(y)} = v_j^{(y)}, \tag{54}$$

$$\dot{v}_j^{(x)} = a_j^{(x)}, \qquad \dot{v}_j^{(y)} = a_j^{(y)}, \tag{55}$$

$$\dot{a}_j^{(x)} = -\frac{1}{\rho}a_j^{(x)} + \frac{1}{\rho}u_j^{(x)}, \qquad \dot{a}_j^{(x)} = -\frac{1}{\rho}a_j^{(x)} + \frac{1}{\rho}u_j^{(x)}, \tag{56}$$

The discrete-time version of the above model in the x-direction can be written as

$$\Delta q_{j,t+1}^{(x)} = \Delta q_{j,t}^{(x)} + \Delta t \cdot v_{j,t}^{(x)} + \left(\rho^2 e^{-\Delta t/\rho} + \rho\Delta t - \rho^2\right) a_{j,t}^{(x)} + \left[\rho^2\left(-e^{-\Delta t/\rho}+1\right) + \Delta t\left(-\rho+\Delta t\right)\right] u_{j,t}^{(x)}, \tag{57}$$

$$v_{j,t+1}^{(x)} = v_{j,t}^{(x)} + \rho\left(1 - e^{-\Delta t/\rho}\right) a_{j,t}^{(x)} + \left[\Delta t + \rho\left(e^{-\Delta t/\rho} - 1\right)\right] u_{j,t}^{(x)}, \tag{58}$$

$$a_{j,t+1}^{(x)} = e^{-\Delta t/\rho} a_{j,t}^{(x)} + \left(1 - e^{-\Delta t/\rho}\right) u_{j,t}^{(x)}, \tag{59}$$

The discrete-time dynamics model in the y-direction can be expressed in the same way and will not be repeated here. Then, the expression for matrix $\mathbf{A}_j$ in equation (9) is given by

$$\mathbf{A}_j = \begin{bmatrix} \mathbf{A}_{j,1} & \mathbf{A}_{j,2} \end{bmatrix}, \tag{60}$$

where

$$\mathbf{A}_{j,1} = \begin{bmatrix} 1 & 0 & 0 & 0 & 0 & 0 \\ 0 & 1 & 0 & 0 & 0 & 0 \\ \Delta t & 0 & 1 & 0 & 0 & 0 \\ 0 & \Delta t & 0 & 1 & 0 & 0 \end{bmatrix}^T, \quad \mathbf{A}_{j,2} = \begin{bmatrix} \rho^2 e^{-\Delta t/\rho} + \rho\Delta t - \rho^2 & 0 \\ 0 & \rho^2 e^{-\Delta t/\rho} + \rho\Delta t - \rho^2 \\ \rho\left(1 - e^{-\Delta t/\rho}\right) & 0 \\ 0 & \rho\left(1 - e^{-\Delta t/\rho}\right) \\ e^{-\Delta t/\rho} & 0 \\ 0 & e^{-\Delta t/\rho} \end{bmatrix}. \tag{61}$$

Similarly, the expression for matrix $\mathbf{B}_j$ can be written as

$$\mathbf{B}_j = \begin{bmatrix} \rho^2\left(-e^{-\Delta t/\rho}+1\right) + \Delta t(-\rho+\Delta t) & 0 & \Delta t+\rho\left(e^{-\Delta t/\rho} - 1\right) & 0 & 1-e^{-\Delta t/\rho} & 0 \\ 0 & \rho^2\left(-e^{-\Delta t/\rho}+1\right) + \Delta t(-\rho+\Delta t) & 0 & \Delta t+\rho\left(e^{-\Delta t/\rho} - 1\right) & 0 & 1-e^{-\Delta t/\rho} \end{bmatrix}^T. \tag{62}$$

For the covariance matrix ($\mathbf{Q}_{\mathbf{w}}$) of process noise ($\mathbf{w}_{j,t}$), it can be expressed as [36]

$$\mathbf{Q}_{\mathbf{w}} = E\left\{\mathbf{w}_{j,t}\mathbf{w}_{j,t}^{T}\right\} = \begin{bmatrix} \mathbf{Q}_{\mathbf{w},1} & \mathbf{0}_{4\times 2} \\ \mathbf{0}_{2\times 4} & \mathbf{Q}_{\mathbf{w},2} \end{bmatrix}, \tag{63}$$

where

$$\mathbf{Q}_{\mathbf{w},1} = \begin{bmatrix} \Delta t^3\varsigma_x^2/3 & 0 & \Delta t^2\varsigma_x^2/2 & 0 \\ 0 & \Delta t^3\varsigma_y^2/3 & 0 & \Delta t^2\varsigma_y^2/2 \\ \Delta t^2\varsigma_x^2/2 & 0 & \Delta t\cdot\varsigma_x^2 & 0 \\ 0 & \Delta t^2\varsigma_y^2/2 & 0 & \Delta t\cdot\varsigma_y^2 \end{bmatrix}^{T}, \quad \mathbf{Q}_{\mathbf{w},2} = \begin{bmatrix} \varsigma_x^2 & 0 \\ 0 & \varsigma_y^2 \end{bmatrix}; \tag{64}$$

Parameters ς_x^2 and ς_y^2 represent the continuous-time acceleration process noise intensity in x- and y-directions, respectively.

APPENDIX B
RELATIONSHIP BETWEEN BLOCKLENGTH AND TRANSMISSION SUCCESS RATE

The air-to-ground (A2G) link between the i-th UAV-B and its corresponding BS is modeled as a Rayleigh fading channel, whose channel power gain is represented by $|h_{i,t}|^2$. Denote the transmit power of UAV-Bs and the noise power at BSs as P_t and N_0, then the SNR of the i-th UAV-B's signal at BS can be expressed as

$$\gamma_{i,t} = (P_t/N_0)\cdot|h_{i,t}|^2, \tag{65}$$

According to [37], if the number of symbols used to transmit the sensing data corresponding to the j-th UAV-A and i-th UAV-B in time slot t is $\theta_{j,t}^i$, the success rate of data transmission can be calculated as

$$P^{(s)}\left(\theta_{j,t}^i, \gamma_{i,t}\right) = 1 - Q\left(f\left(\theta_{j,t}^i, \gamma_{i,t}\right)\right), \tag{66}$$

where $Q(x) = (2\pi)^{-1/2}\int_x^\infty e^{-z^2/2}dz$, and

$$f\left(\theta_{j,t}^i, \gamma_{i,t}\right) = \ln(2)\sqrt{\frac{\theta_{j,t}^i}{V_{i,t}}}\cdot\left[\log_2(1+\gamma_{i,t}) - \frac{D}{\theta_{j,t}^i}\right]; \tag{67}$$

D is the size of sensing data (bits) and $V_{i,t} = 1-(1+\gamma_{i,t})^{-2}$.

Conversely, for a given success rate $P_{j,t}^{i,(s)}$ ($P_{j,t}^{i,(s)} \geq 0.5$), the minimum number of symbols required for data transmission is given by

$$\theta\left(P_{j,t}^{i,(s)}, \gamma_{i,t}\right) = 2D \cdot \left\{ \frac{V_{i,t}}{D} \cdot \left(\frac{Q^{-1}\left(1-P_{j,t}^{i,(s)}\right)}{\ln(2)} \right)^2 + 2\log_2(1+\gamma_{i,t}) - \left[\frac{V_{i,t}^2}{D^2} \cdot \left(\frac{Q^{-1}\left(1-P_{j,t}^{i,(s)}\right)}{\ln(2)} \right)^4 + 4\log_2(1+\gamma_{i,t}) \left(\frac{V_{i,t}}{D}\right) \left(\frac{Q^{-1}\left(1-P_{j,t}^{i,(s)}\right)}{\ln(2)} \right)^2 \right]^{\frac{1}{2}} \right\}^{-1}, \qquad P_{j,t}^{i,(s)} \geq 0.5. \tag{68}$$

APPENDIX C
PROOF OF PROPOSITION 1

According to equations (42), (43) and (47), $\sigma_{\Delta\mathbf{q},m}^2 \cdot \mathbf{I}_{N_A^U} - \bar{\mathbf{D}}_{\Delta\mathbf{q},m,t+1}(\boldsymbol{\varphi}_t, \boldsymbol{\theta}_t)$ is a diagonal matrix. Thus, we have

$$\begin{aligned} &\mathrm{tr}\left(\mathbf{S}(\mathbf{p}_m)\left(\sigma_{\Delta\mathbf{q},m}^2 \cdot \mathbf{I}_{N_A^U} - \bar{\mathbf{D}}_{\Delta\mathbf{q}.m,t+1}(\boldsymbol{\varphi}_t, \boldsymbol{\theta}_t)\right)\mathbf{S}(\mathbf{p}_m)^T\right) \\ &\qquad = \sum_{l=1}^{2} \mathbf{s}_l(\mathbf{p}_m)\left(\sigma_{\Delta\mathbf{q},m}^2 \cdot \mathbf{I}_{N_A^U} - \bar{\mathbf{D}}_{\Delta\mathbf{q},m,t+1}(\boldsymbol{\varphi}_t, \boldsymbol{\theta}_t)\right)\mathbf{s}_l(\mathbf{p}_m)^T, \end{aligned} \tag{69}$$

where $\mathbf{s}_l(\mathbf{p}_m)$ represents the l-th row vector of matrix $\mathbf{S}(\mathbf{p}_m)$. Moreover, if condition (46) is satisfied, the elements in diagonal matrix $\sigma_{\Delta\mathbf{q},m}^2 \cdot \mathbf{I}_{N_A^U} - \bar{\mathbf{D}}_{\Delta\mathbf{q},m,t+1}(\boldsymbol{\varphi}_t, \boldsymbol{\theta}_t)$ are all non-negative, which means that it is a positive semi-definite (PSD) matrix. According to the definition of PSD matrices, we have

$$\mathbf{s}_l(\mathbf{p}_m)\left(\sigma_{\Delta\mathbf{q},m}^2 \cdot \mathbf{I}_{N_A^U} - \bar{\mathbf{D}}_{\Delta\mathbf{q}.m,t+1}(\boldsymbol{\varphi}_t, \boldsymbol{\theta}_t)\right)\mathbf{s}_l(\mathbf{p}_m)^T \geq 0. \tag{70}$$

Then, the following inequality holds:

$$\mathrm{tr}\left(\mathbf{S}(\mathbf{p}_m)\left(\sigma_{\Delta\mathbf{q},m}^2 \cdot \mathbf{I}_{N_A^U} - \bar{\mathbf{D}}_{\Delta\mathbf{q}.m,t+1}(\boldsymbol{\varphi}_t, \boldsymbol{\theta}_t)\right)\mathbf{S}(\mathbf{p}_m)^T\right) \geq 0. \tag{71}$$

Finally, we have

$$\begin{aligned} \mathrm{tr}\left(\mathbf{S}(\mathbf{p}_m)\bar{\mathbf{D}}_{\Delta\mathbf{q}.m,t+1}(\boldsymbol{\varphi}_t, \boldsymbol{\theta}_t)\mathbf{S}(\mathbf{p}_m)^T\right) &\leq \mathrm{tr}\left(\mathbf{S}(\mathbf{p}_m)\left(\sigma_{\Delta\mathbf{q},m}^2 \cdot \mathbf{I}_{N_A^U}\right)\mathbf{S}(\mathbf{p}_m)^T\right) \\ &= \sigma_{\Delta\mathbf{q},m}^2 \cdot \mathrm{tr}\left(\mathbf{S}(\mathbf{p}_m)\mathbf{S}(\mathbf{p}_m)^T\right) = \sigma_{\Delta\mathbf{q},m}^2 \cdot \mathrm{tr}\left(\mathbf{P}(\mathbf{p}_m)\right) = Thr_m. \end{aligned} \tag{72}$$

This completes the proof of Proposition 1.

REFERENCES

[1] R. Keating, M. Säily, J. Hulkkonen, and J. Karjalainen, "Overview of positioning in 5G new radio," in *2019 16th International Symposium on Wireless Communication Systems (ISWCS)*, 2019, pp. 320–324.

[2] S. Dang, O. Amin, B. Shihada, and M.-S. Alouini, "What should 6G be?" *Nature Electronics*, vol. 3, no. 1, pp. 20–29, 2020.

[3] D. Lu, S. Jiang, B. Cai, W. Shangguan, K. Liu, and J. Luan, "Quantitative analysis of GNSS performance under railway obstruction environment," in *2018 IEEE/ION Position, Location and Navigation Symposium (PLANS)*, 2018, pp. 1074–1080.

[4] Q. Liu, R. Liu, Z. Wang, and Y. Zhang, "Simulation and analysis of device positioning in 5G ultra-dense network," in *2019 15th International Wireless Communications & Mobile Computing Conference (IWCMC)*, 2019, pp. 1529–1533.

[5] B. Xu, Q. Jia, and L.-T. Hsu, "Vector tracking loop-based GNSS NLOS detection and correction: Algorithm design and performance analysis," *IEEE Transactions on Instrumentation and Measurement*, vol. 69, no. 7, pp. 4604–4619, 2020.

[6] K. Shamaei and Z. M. Kassas, "LTE receiver design and multipath analysis for navigation in urban environments," *NAVIGATION*, vol. 65, no. 4, pp. 655–675, 2018.

[7] Y. Zeng, Q. Wu, and R. Zhang, "Accessing from the sky: A tutorial on UAV communications for 5G and beyond," *Proceedings of the IEEE*, vol. 107, no. 12, pp. 2327–2375, 2019.

[8] Z. Wang, R. Liu, Q. Liu, L. Han, J. S. Thompson, Y. Lin, and W. Mu, "Toward reliable UAV-enabled positioning in mountainous environments: System design and preliminary results," *IEEE Transactions on Reliability*, pp. 1–29, 2021.

[9] G. Han, J. Jiang, C. Zhang, T. Q. Duong, M. Guizani, and G. K. Karagiannidis, "A survey on mobile anchor node assisted localization in wireless sensor networks," *IEEE Communications Surveys & Tutorials*, vol. 18, no. 3, pp. 2220–2243, 2016.

[10] Z. Wang, R. Liu, Q. Liu, J. S. Thompson, and M. Kadoch, "Energy-efficient data collection and device positioning in UAV-assisted IoT," *IEEE Internet of Things Journal*, vol. 7, no. 2, pp. 1122–1139, 2020.

[11] S. Zhang, R. Pöhlmann, E. Staudinger, and A. Dammann, "Assembling a swarm navigation system: Communication, localization, sensing and control," in *2021 IEEE 18th Annual Consumer Communications & Networking Conference (CCNC)*, 2021, pp. 1–9.

[12] G. Zhao, M. A. Imran, Z. Pang, Z. Chen, and L. Li, "Toward real-time control in future wireless networks: Communication-control co-design," *IEEE Communications Magazine*, vol. 57, no. 2, pp. 138–144, 2019.

[13] K. Meng, Q. Wu, S. Ma, W. Chen, and T. Q. S. Quek, "UAV trajectory and beamforming optimization for integrated periodic sensing and communication," *IEEE Wireless Communications Letters*, pp. 1–1, 2022.

[14] M. Eisen, M. M. Rashid, K. Gatsis, D. Cavalcanti, N. Himayat, and A. Ribeiro, "Control aware radio resource allocation in low latency wireless control systems," *IEEE Internet of Things Journal*, vol. 6, no. 5, pp. 7878–7890, 2019.

[15] C. De Lima *et al.*, "Convergent communication, sensing and localization in 6G systems: An overview of technologies, opportunities and challenges," *IEEE Access*, vol. 9, pp. 26 902–26 925, 2021.

[16] Y. Zeng, Q. Wu, and R. Zhang, "Accessing from the sky: A tutorial on UAV communications for 5G and beyond," *Proceedings of the IEEE*, vol. 107, no. 12, pp. 2327–2375, 2019.

[17] N. Zhao, W. Lu, M. Sheng, Y. Chen, J. Tang, F. R. Yu, and K.-K. Wong, "UAV-assisted emergency networks in disasters," *IEEE Wireless Communications*, vol. 26, no. 1, pp. 45–51, 2019.

[18] N. Zhao, F. Cheng, F. R. Yu, J. Tang, Y. Chen, G. Gui, and H. Sari, "Caching UAV assisted secure transmission in hyper-dense networks based on interference alignment," *IEEE Transactions on Communications*, vol. 66, no. 5, pp. 2281–2294, 2018.

[19] H. Sallouha, M. M. Azari, A. Chiumento, and S. Pollin, "Aerial anchors positioning for reliable RSS-based outdoor localization in urban environments," *IEEE Wireless Communications Letters*, vol. 7, no. 3, pp. 376–379, 2018.

[20] H. Sallouha, M. M. Azari, and S. Pollin, "Energy-constrained UAV trajectory design for ground node localization," in *2018 IEEE Global Communications Conference (GLOBECOM)*, 2018, pp. 1–7.

[21] Z. Wang, R. Liu, Q. Liu, L. Han, and J. S. Thompson, "Feasibility study of UAV-assisted anti-jamming positioning," *IEEE Transactions on Vehicular Technology*, pp. 1–1, 2021.

[22] Q. Liu, R. Liu, Z. Wang, and J. S. Thompson, "UAV swarm-enabled localization in isolated region: A rigidity-constrained deployment perspective," *IEEE Wireless Communications Letters*, pp. 1–1, 2021.

[23] D. Xu, Y. Sun, D. W. K. Ng, and R. Schober, "Multiuser MISO UAV communications in uncertain environments with no-fly zones: Robust trajectory and resource allocation design," *IEEE Transactions on Communications*, vol. 68, no. 5, pp. 3153–3172, 2020.

[24] Y. Liu, Y. Wang, J. Wang, and Y. Shen, "Distributed 3D relative localization of UAVs," *IEEE Transactions on Vehicular Technology*, vol. 69, no. 10, pp. 11 756–11 770, 2020.

[25] F. Liu, C. Masouros, A. P. Petropulu, H. Griffiths, and L. Hanzo, "Joint radar and communication design: Applications, state-of-the-art, and the road ahead," *IEEE Transactions on Communications*, vol. 68, no. 6, pp. 3834–3862, 2020.

[26] W. Yuan, F. Liu, C. Masouros, J. Yuan, D. W. K. Ng, and N. González-Prelcic, "Bayesian predictive beamforming for vehicular networks: A low-overhead joint radar-communication approach," *IEEE Transactions on Wireless Communications*, vol. 20, no. 3, pp. 1442–1456, 2021.

[27] J. Mei, K. Zheng, L. Zhao, L. Lei, and X. Wang, "Joint radio resource allocation and control for vehicle platooning in LTE-V2V network," *IEEE Transactions on Vehicular Technology*, vol. 67, no. 12, pp. 12 218–12 230, 2018.

[28] A. González, N. Franchi, and G. Fettweis, "Control loop aware LTE-V2X semi-persistent scheduling for string stable CACC," in *2019 IEEE 30th Annual International Symposium on Personal, Indoor and Mobile Radio Communications (PIMRC)*, 2019, pp. 1–7.

[29] Y. Wu, Q. Yang, H. Li, K. S. Kwak, and V. C. M. Leung, "Control-aware energy-efficient transmissions for wireless control systems with short packets," *IEEE Internet of Things Journal*, vol. 8, no. 19, pp. 14 920–14 933, 2021.

[30] X. Shi, A. Wang, G. Sun, J. Li, and X. Zheng, "Air to air communications based on UAV-enabled virtual antenna arrays: A multi-objective optimization approach," in *2022 IEEE Wireless Communications and Networking Conference (WCNC)*, 2022, pp. 878–883.

[31] Y. Cai, X. Jiang, M. Liu, N. Zhao, Y. Chen, and X. Wang, "Resource allocation for URLLC-oriented two-way UAV relaying," *IEEE Transactions on Vehicular Technology*, vol. 71, no. 3, pp. 3344–3349, 2022.

[32] S. Frattasi and F. Della Rosa, *Mobile positioning and tracking: from conventional to cooperative techniques*. John Wiley & Sons, 2017.

[33] K. C. Ho, X. Lu, and L. Kovavisaruch, "Source localization using TDOA and FDOA measurements in the presence of receiver location errors: Analysis and solution," *IEEE Transactions on Signal Processing*, vol. 55, no. 2, pp. 684–696, 2007.

[34] W. H. FOY, "Position-location solutions by Taylor-series estimation," *IEEE Transactions on Aerospace and Electronic Systems*, vol. AES-12, no. 2, pp. 187–194, 1976.

[35] C. Dussault, R. Courtois, J.-P. Ouellet, and J. Huot, "Influence of satellite geometry and differential correction on GPS location accuracy," *Wildlife Society Bulletin*, vol. 29, no. 1, pp. 171–179, 2001.

[36] S. Ragothaman, M. Maaref, and Z. M. Kassas, "Multipath-optimal UAV trajectory planning for urban UAV navigation with cellular signals," in *2019 IEEE 90th Vehicular Technology Conference (VTC2019-Fall)*, 2019, pp. 1–6.

[37] C. Pan, H. Ren, Y. Deng, M. Elkashlan, and A. Nallanathan, "Joint blocklength and location optimization for URLLC-enabled UAV relay systems," *IEEE Communications Letters*, vol. 23, no. 3, pp. 498–501, 2019.